



The influence of the geometrical features on the seismic response of historical churches reinforced by different cross lam roof-solutions

Nicola Longarini¹ · Pietro Crespi¹ · Marco Zucca¹

Received: 28 December 2021 / Accepted: 26 June 2022
© The Author(s) 2022

Abstract

Recent Italian earthquakes have shown the seismic vulnerability of many typical historical masonry churches characterized by one nave and wooden roofs. Under transverse earthquake, the nave transverse response of this kind of churches can be influenced by the geometrical and material features. To increase the seismic performance, strengthening interventions aimed to pursue the global box-behavior by the realization of dissipative roof-structure represent a valid strategy, especially to avoid out-of-plane mechanisms. In this way, the roof structure must be able to represent a tool for the damped rocking of the perimeter walls. Cross-laminated timber (CLT) panels with calibrated metal connections have been recently adopted in experimental tests as a valid solution to obtain a roof-diaphragm with ductile behavior, satisfying the conservative restoration criteria at the same time. In this paper, after a description of the numerical approach for the damped rocking mechanism for one nave configuration church, the effectiveness of different CLT based roof-diaphragms in the nave transverse response is investigated for four historical churches. The seismic responses are performed by comparative dynamic nonlinear analyses and the results are shown in terms of displacements and shear actions transferred to the façade. The influence of the geometrical features of the churches on the nave transversal response is deepened by sensitivity analyses with the aim to predict the displacements and shear variations under the same earthquake excitation.

Keywords Cross-laminated timber roof · Historical masonry churches · Seismic retrofitting · Nave transverse response · Rocking failure

✉ Nicola Longarini
nicola.longarini@polimi.it

Pietro Crespi
pietro.crespi@polimi.it

Marco Zucca
marco.zucca@polimi.it

¹ Department of Architecture, Built Environment and Construction Engineering, Politecnico di Milano, Milan, Italy

1 Introduction

The seismic preservation of the construction heritage is a crucial task for the human life protection and for social-economic-historical roles represented by masonry buildings in Historical centers (Valluzzi et al. 2021), churches (Valente and Milani 2018a; Valente and Milani 2018b; Valente and Milani 2018c), basilicas (Zucca et al. 2018, 2020; Fazzi et al. 2021) and towers (Pavia et al. 2021; Kita et al. 2021). These buildings, built in areas only nowadays classified as seismic (Valente and Milani 2018a), must be preserved from the future earthquake's effects to avoid possible failures and collapses like the ones occurred for instance in Italy during the last century: Sicily (1908), Irpinia and Vulture (1930), Belice (1968), Friuli (1976), Irpinia (1980), Carlentini (1990), Umbria and Marche (1997), Molise (2002), Abruzzo (2009), Emilia-Romagna (2012), Marche and Abruzzo (2016), and Ischia (2017). Among the historical constructions, this paper is focused on the seismic behavior of the one-nave masonry churches characterized by wooden roof. For this kind of construction, the observation of post-earthquake damages allowed the identification of several recurring collapse mechanisms (Benedetti and Castellani 1981; Milani 2013, Sorrentino et al. 2019). The seismic vulnerability, inducing partial damages or overall collapse, depends on the materials and building typologies (Dal Cin and Russo 2016; Fazzi et al. 2021). In fact, the seismic response is strictly related to the geometric characteristics (De Matteis et al. 2017) of these constructions. For the one-nave churches, the nave transverse response (Martinez et al. 2006; Roque et al. 2019) mainly induces both out-of-plane rocking mechanisms of the perimeter walls and excessive in-plane stresses on the seismic resistant elements transversally positioned with the longitudinal axis of the church (triumphal arches, head wall, head gable, etc.), (Giuriani et al. 2016; Valente and Milani 2018b). Therefore, to improve the seismic performance, the global box behavior must be pursued by adopting idoneous retrofitting techniques able to respect, as far as possible, the authenticity of the construction (Longarini et al. 2019, Mibact 2010). Among these techniques, perimeter and transversal chains can be adopted (De Matteis et al. 2017) even if its efficiency, in nave transversal response, can be jeopardized in case of poor-quality masonry or high slenderness of the perimeter walls. Recently, the realization of dissipative wooden roof-diaphragm represents another valid option to avoid the out-of-plane mechanisms and to reduce the in-plane shear actions on the seismic resistant elements (Longarini et al. 2019), obtaining a controlled rocking behavior of the perimeter walls opportunely coupled with the dissipative roof-diaphragm. The diaphragm can be realized with wooden planks having different orientation with respect to the original one (Parisi and Piazza 2015) or by precast solution of Cross Laminated Timber (CLT) panels overlaying the original wooden trusses and planks and creating wood-to-wood composite sections (Gubana 2010; Gubana 2015, Roensmaens 2019). In several experimental tests and numerical analyses, the system composed by CLT panels with steel connections has provided adequate in-plane stiffness able to guarantee the floor diaphragm effect (Gubana and Melotto 2018; Longarini et al. 2018). The roof diaphragm should be optimized according to the thickness of the panels and the typology and numerosity of the steel connections. Therefore, the nave transversal response, influenced by the church's materials and geometries, also depends on the CLT panel thickness, the features of the panel-to-panel, and walls-to-panels connections (i.e. connectors diameter, numbers and spacing). The roof-diaphragm solution able to improve the seismic response should be calibrated in terms of its strength and stiffness: the system characterized by the panels and the connections must be able to withstand in-plane shear actions by dissipating the seismic energy in the connections. On the contrary, a rigid

and stiff typology of connections can produce excessive in-plane shear on the CLT. Consequently, the increase of the panels' thickness appears mandatory also causing a change in global seismic response due to the structural mass increase. Four one-nave churches are here analyzed to perform comparative analyses among churches with the same configuration and geometries; comparative analyses about the seismic response for historical buildings or churches similar themselves represent a valid approach to predict as far as possible the seismic behavior and to highlight the best structural retrofitting technique as it is performed for long-span historical structures in (Roca and Clemente 2005), basilica churches in (Brandonisio et al. 2008; Betti et al. 2018; Lucibello et al. 2010), medieval churches in (Valente et al. 2017), unreinforced masonry buildings with flexible diaphragms in (Betti et al. 2014), historical masonry churches located in the same historical Center in (Valente and Milani 2018c), Benedictine Basilica typology in (Fazzi et al. 2021). These analyses consider the same seismic action but different CLT roof-diaphragm solutions and evaluate the influence of the panels' thickness and connection stiffness. For each church strengthened by the CLT roof diaphragm configurations, sensibility analyses are carried out for detecting the importance of the following geometrical features on the seismic response: the geometrical slenderness of the perimeter walls, the geometrical slenderness of the façade and the ratio between length and width of the churches (shape factor). The dynamic analyses (where the seismic action is represented through a set of seven spectrum-compatible accelerograms) are performed by adopting equivalent models in which the nonlinear material properties of the masonry are introduced by means of rotational inelastic hinges located at the base of the equivalent vertical elements, while the nonlinear properties of the roof are introduced through shear inelastic hinges located in the equivalent horizontal elements (Giuriani and Marini 2008; Preti et al. 2017). This method is based on the structure discretization by macro-elements, with concentrated nonlinear properties (Pagnoni 1994; Lourenço et al. 1995; Lagomarsino et al. 2013).

The paper is organized as follows: (i) the numerical approach for the damped rocking schematization of one nave masonry churches with wooden roof structure is described in Sect. 2, (ii) the general issues of the sensitivity analyses are discussed in Sect. 3 together with the results of the sensitivity analysis and the relative remarks, (iii) general conclusions are finally presented in Sect. 4.

2 Numerical approach for the damped rocking schematization

2.1 Equivalent model

The nonlinear dynamic analyses can be performed with equivalent finite element models (EQ_FEM) in which mono-dimensional macro-elements represent the parts of the church involved in the nave transversal response. The transversal seismic resistant systems of the church (façade, coupled lateral walls, triumphal arches, head wall) are initially selected along the longitudinal axis in order to realize the model of the church (Fig. 1). Nonlinear properties of the perimeter masonry walls and CLT roof diaphragm can be assigned to the equivalent elements (Giuriani and Marini 2008).

In order to implement the EQ_FEM the following three steps can be followed:

(i) in the first step, preliminary pushover analyses are carried out on sub-structures representing the single parts of the n-seismic resistant systems, i.e. the piers of the longitudinal

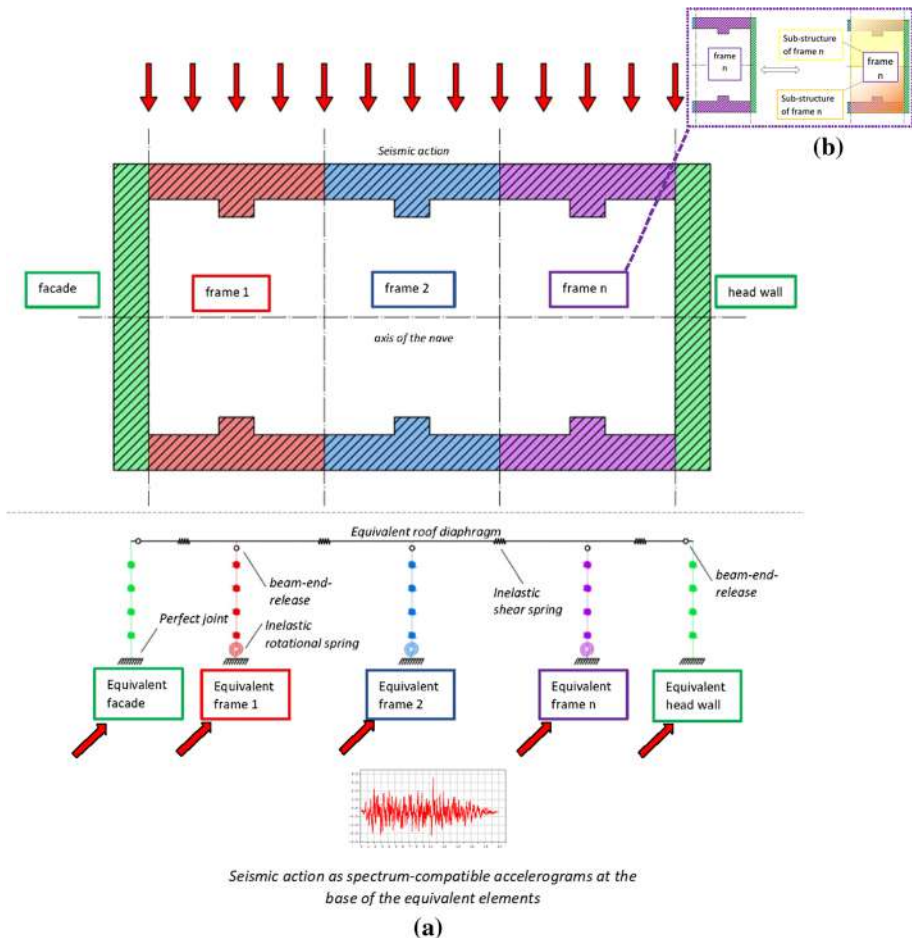


Fig. 1 **a** Example of seismic resistant frame identification for one nave configuration church (plan view) and related equivalent finite element model representation (longitudinal view): the façade and the head wall are identified in green; the seismic resistant frames are identified in red, blue and violet; the roof-diaphragm is identified in grey; **b** Identification (plan view) of the sub-structures characterizing the n-seismic resistant frame; the two sub-structures are identified respectively in yellow and orange

walls included between the openings or the abutments (Figs. 1 and 2a). Each sub-structure is divided in sections with fibers discretization where the nonlinear properties are assigned to the fibers by adopting the concrete trilinear model with zero tensile resistance (Midas 2021), or considering the concrete damaged plasticity model (Lubliner et al. 1989; Lee and Fenves 2002) in which tensile cracking and compressive crushing are the main failure modes (Milani et al. 2018);

(ii) in the second step, on the basis of the preliminary results obtained in the pushover analyses of the first step, the yielding and ultimate values of the $M-\chi$ diagram of the various members are assigned to the base sections of each equivalent seismic resistant system as bi-linear inelastic rotational springs. Then, pushover analyses are performed again detecting the shear-displacement curves of the transverse resistant system. Consequently, the $M-\chi$ diagrams of each system are obtained by multiplying and dividing the

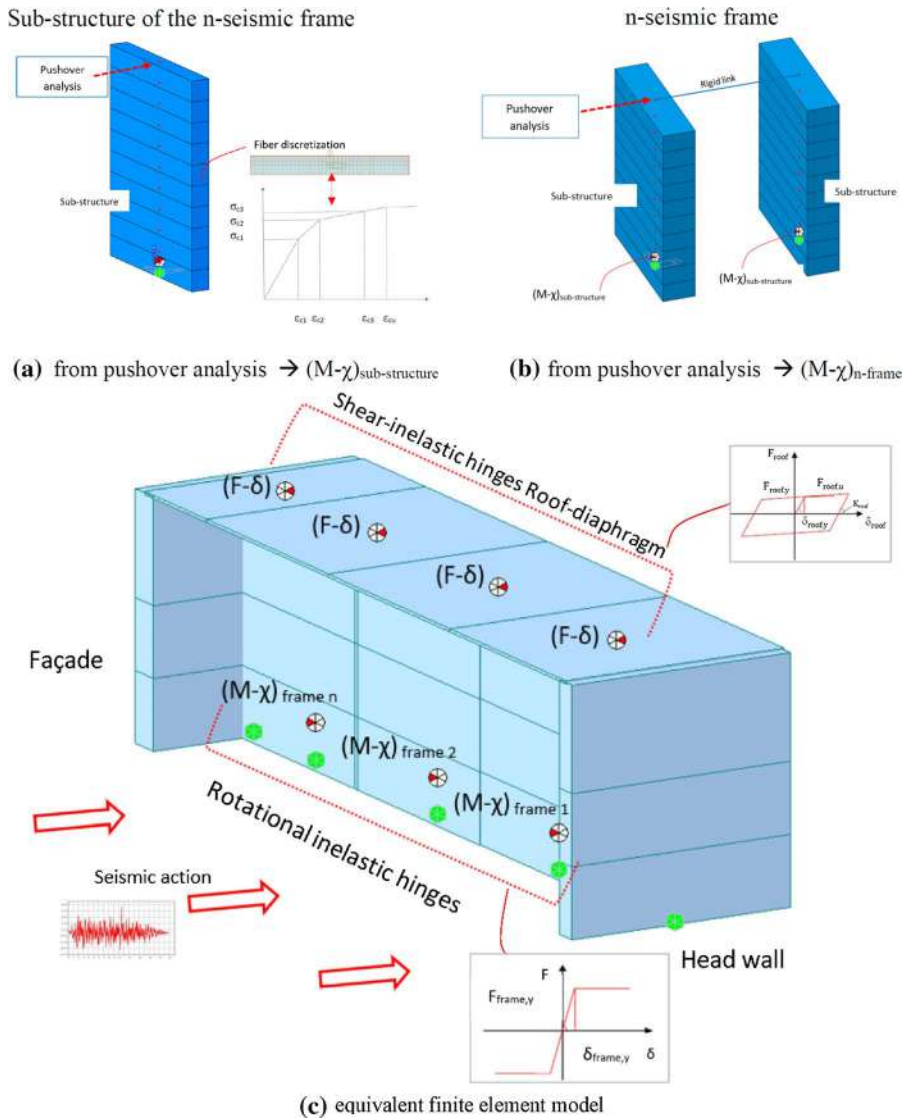


Fig. 2 steps for the EQ_FEM implementation—**a** pushover analyses on sub structures of the seismic resistant frames with fibers discretization with concrete trilinear model assigned to the fibers—**b** pushover analyses on seismic resistant frame with inelastic rotational springs having $M-\chi$ detected in the previous step—**c** view of the equivalent finite element model (EQ_FEM) to be analyzed under seven spectrum compatible accelerograms

shear-displacements curves for the shear length (Figs. 1 and 2b), considering the distance between the section with zero bending moment and the section with maximum bending moment.

(iii) In the third step, the head wall, the façade and the transverse frames are modeled as vertical mono-dimensional equivalent elements. Typically, the façade and the head wall have in-plane strength and stiffness greater than the longitudinal walls, thus these

structural members are implemented by equivalent elastic mono-dimensional elements fully restrained at the base (Giuriani and Marini 2008; Preti et al. 2014). Instead, the transverse frames have concentrated inelastic rotational springs at the base described by $M-\chi$ diagrams obtained by the pushover analyses performed in the second step (Fig. 2c). In this third step, the EQ_FEM is completed by the introduction of horizontal mono-dimensional equivalent elements representing the roof-diaphragm (Preti et al. 2017). The elements of the roof are linked to the vertical ones by hinges located at the end of the vertical elements. This kind of implementation allows to trigger the rocking and to release the bending moment transferred to the roof. The equivalent elements of the roof are also pinned with respect to the head wall and façade. The roof's shear deformability and the nonlinear behavior of the connections are also introduced to ensure the dissipative response of the roof diaphragm by means of shear elastic-plastic hinges. The shear roof springs can be described by the trilinear degrading model (Ferreira et al. 2014) or by the Clough model (Genshu and Yongfeng 2007; Rinaldin et al. 2013; Gavric et al. 2015; Hossain et al. 2015; Preti et al. 2017) in which the unloading stiffness is obtained reducing the elastic one according to the general Eq. (1):

$$K_R = K_0 \left| D_y / D_m \right|^\alpha \leq K_0 \quad (1)$$

where K_R is the unloading stiffness, K_0 is the elastic stiffness, D_y is the yield displacement, D_m is the maximum displacement and α is the unloading stiffness degradation parameter, assumed equal to 0.4 (Otani 1981). The unloading stiffness gradually reduces when the deformation increases.

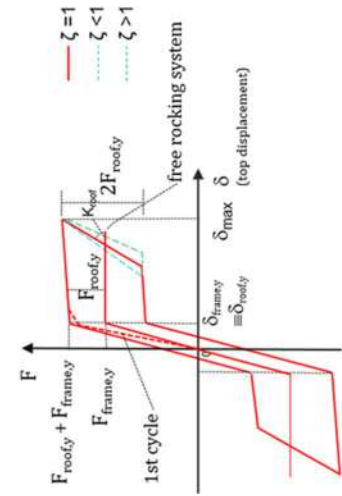
As mentioned before, the earthquake is represented by a set of spectrums compatible accelerograms acting perpendicularly to the nave axis (Fig. 2c).

2.2 Damped rocking response

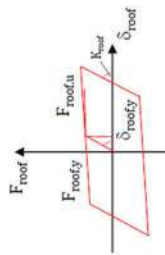
The CLT panels together with the wall-to-roof and wall-to-wall connections represent a deformable diaphragm able to permit the rocking trigger of the perimeter walls, limiting either the lateral displacements (within a fixed design range) and the seismic loads on the rigid head walls (thanks to the energy dissipation occurred in the steel connections). The dissipative roof-diaphragm works as a damper located at the top of the construction (Bolis et al. 2013).

Thanks to the dissipative roof-diaphragm, the nave transversal response of one nave historical churches, usually characterized by a high percentage of the total mass involved in the first vibrational mode, can be represented by a flag-shaped diagram (Fig. 3c) given by (i) the bi-linear free rocking behavior of the masonry seismic resistant systems (Fig. 3a) (Bolis et al. 2013; Preti et al. 2017) and the (ii) dissipative hysteretic behavior of the roof-diaphragm induced by the nonlinear behavior of the connections (Fig. 3b), (Johansen 1949; Larsen 1977; Tomasi et al. 2010; Marini et al. 2018; Longarini et al. 2019). Figure 3 is adapted from Preti et al. 2017.

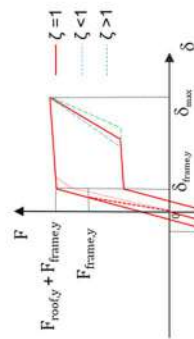
The bi-linear behavior of the free rocking can be described by the yielding and ultimate force (respectively $F_{frame,y}$ and $F_{frame,u}$) related to the yielding and the ultimate displacements of the generic resistant seismic frame (respectively $\delta_{frame,y}$ and $\delta_{frame,u}$). These values come out from the pushover analyses of the second step already described



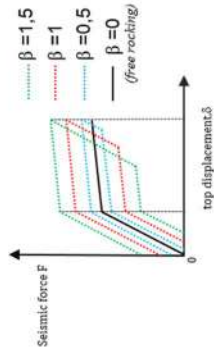
(a) Free rocking system



(b) Elastic-plastic roof diaphragm



(c) Flag shaped diagram of the dissipative rocking



(d) Variation of the flag shaped capacity curve for β variation

(e) Damped rocking when the rocking activation's displacement differs from the roof's yielding displacement

Fig. 3 dumped rocking diagram, (adapted from Preti et al. 2017)

in Sect. 2.1 (Figs. 1 and 2a). The stiffness of the frame is consequently given by the ratio $k_{frame} = F_{frame,y} / \delta_{frame,y}$.

Similarly, the dissipative behavior of the roof can be described by the yielding and the ultimate force (respectively $F_{roof,y}$ and $F_{roof,u}$) related to the yielding and the ultimate displacements of the roof (respectively $\delta_{roof,y}$ and $\delta_{roof,u}$). These values can be determined from experimental tests on the connectors chosen for the connections (Sandhaas and Van de Kuilem 2017; Gavric et al. 2015). The stiffness of the roof is consequently given by the ratio $k_{roof} = F_{roof,y} / \delta_{roof,y}$. Referring to Fig. 3c, the flag shaped diagram is mainly described by two hysteretic variables ζ and β , respectively:

$$\zeta = \frac{(F_{roof,y} k_{frame})}{(F_{frame,u} k_{roof})} \quad (2)$$

$$\beta = 2 \frac{F_{roof,y}}{F_{frame,y}} \quad (3)$$

therefore, the yielding force of the roof can be expressed in terms of β , Eq. (4), while the stiffness of the roof can be expressed by ζ and β , respectively Eqs. (5) and (6):

$$F_{roof,y} = \frac{(F_{frame,y} \beta)}{2} \quad (4)$$

$$k_{roof,y} = \frac{(k_{frame} F_{roof,y})}{(\zeta F_{frame,y})} \quad (5)$$

$$k_{roof,y} = k_{frame,y} \frac{\beta \delta_{frame,y}}{2 \delta_{roof,y}} \quad (6)$$

It is remarkable that:

- ζ can be also described by the ratio between the yielding displacements of the roof and the yielding displacements of the frame ($\zeta = \delta_{roof,y} / \delta_{frame,y}$). It gives a measure of the roof-diaphragm stiffness, and it is indirectly proportional to k_{roof} because if ζ increases, lower energy dissipation occurs (Fig. 3d);
- β is the key parameter for the intervention design being an index of the energy dissipated by the roof: if β increases, the damping effect increases too (Fig. 3e). Therefore, it must be calibrated in the preferable range $\beta = 0 \div 1.5$; in fact, $\beta < 2$ is preferable because it allows the self-centering rocking behavior whereas for $\beta > 2$ the re-centering property is partially inhibited having a flag-shaped diagram with significant residual displacements (Fig. 3e, the diagram changes from the blue line to the green one);
- the stiffness of the roof diaphragm k_{roof} characterized by the wood elements and the steel connections can be evaluated by considering the bending stiffness k_{df} and the shear one k_{dt} as it is noted in Eq. (7) where the equivalent elastic modulus E_w^* , the equivalent shear modulus G_w^* and the ideal inertia moment of the section J_{id}^* are given by Eqs. (8), (9) and (10) (Giuriani and Marini 2008):

$$k_{roof} = \left(\frac{1}{k_{df}} + \frac{1}{k_{dt}} \right)^{-1} = \left(\frac{5}{6} \frac{L^3}{E_w^* J_{id}} \frac{L}{G_w^* A^*} \right)^{-1} \quad (7)$$

$$E_w^*(n_n, n_s) = \frac{\frac{L k_n}{n_s}}{2 \frac{\frac{t_w L_y}{\cos \alpha}}{n_n} + \frac{k_n \cdot \frac{L}{n_s}}{E_w}}; \quad (8)$$

$$G_w^*(n_n, n_s) = \frac{\frac{L \cdot k_n}{n_s}}{2 \cdot \frac{\frac{t_w L_y}{\cos \alpha}}{n_n} + \frac{k_n \cdot \frac{L}{n_s}}{G_w}}; \quad (9)$$

$$J_{id}(n_n, n_s) = \frac{t_w \cdot L_y^3}{12 \cos \alpha} + n_{ws} \cdot \left[2 A_s \left(\frac{L_y}{2} \right)^2 \right] \quad (10)$$

where n_{ws} is the homogenization coefficient of the connection steel to the wooden diaphragm, given by $n_{ws} = E_s / E_w^*$ (where E_s is the steel elastic modulus); L is the distance between the seismic resistant elements (transversely disposed with respect to the central nave); L_y is the width of the roof; i is the spacing of the connectors; k_n is the stiffness of a single connector; t_w is the thickness of the wooden panels; $\chi = 6/5 \cdot \cos^2 \alpha$ is the shear factor of the section ($\chi = 1.2$ for rectangular sections); A_w is the cross-section area of the roof-diaphragm; A^* is the shear area given by Eq. (11):

$$A^* = \frac{A_w}{\chi} = \frac{\frac{t_w L_y}{\cos \alpha}}{\frac{6}{5 \cos^2 \alpha}}; \quad (11)$$

n_n is the number of the connectors for each connection stripe (the ratio between the spacing of the seismic elements and the spacing of the connectors); n_s is the number of the connection stripes for each span; A_s is the cross-section area of the thin steel stripes of the roof diaphragm.

Initial stiffness of the roof k_{roof} depends on the geometrical and material properties of CLT panels and connections and can be evaluated on the basis of preliminary seismic actions estimation as reported in (Giuriani and Marini 2008). The initial k_{roof} can be used in the dynamic nonlinear analyses even if the optimum roof stiffness ($k_{roof-opt}$) could be consequently adjusted in correspondence to optimal β (β_{opt}) able to limit the lateral displacement below the design value (δ_{design}). The design limit displacement can be fixed as $\delta_{design} \leq 0.005 \cdot h_w$, where h_w is the height of the perimeter walls (Giuriani and Marini, 2008). Referring to the damped rocking mechanism (Fig. 3c), it is worth nothing that $k_{roof-opt}$ can be also expressed by Eq. (12) where Δ is the ratio between the yielding displacements of the roof and the frame.

$$k_{roof-opt} = \frac{\beta_{opt} \cdot k_{frame}}{2 \cdot \Delta} \text{ with } \Delta = \frac{\delta_{roof,y}}{\delta_{frame,y}} \quad (12)$$

This kind of approach is valid because the displacement limitation is the first step towards the evaluation of the roof-diaphragm effectiveness (Giuriani et al. 2009, 2016;

Preti et al. 2014). Furthermore, the stiffness of the roof-diaphragm does not influence the intensity of the seismic action on the structure, vice-versa it affects the maximum lateral displacement.

3 Sensitivity analyses

3.1 Aims of the analyses

The aims of the analyses are the evaluation of the effectiveness of CLT panel roof structure on the nave transversal response for historical one nave masonry churches and the evaluation of the influence of the churches' geometrical features on the seismic performance of the churches, for each one of the CLT panel roof structure configurations considered. The case studies (four historical churches) and the CLT panel configurations are described in paragraph 3.2 while the geometrical features considered are the following:

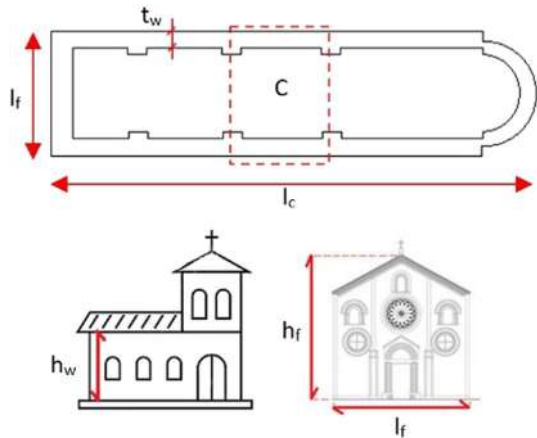
- C is the number of the spans;
- l_c is the length of the church;
- l_f is the width of the church (equal to the façade's dimension along the transversal axis of the church);
- t_w is the average thickness of the lateral walls (their dimension along the transversal axis of the church);
- h_w is the height of the lateral walls;
- λ_w is the geometrical slenderness of the walls given by the ratio $\lambda_w = h_w/t_w$;
- h_f is the height of the façade;
- λ_f is the geometrical slenderness of the façade given by the ratio $\lambda_f = h_f/l_f$;
- S_F is the shape factor of the church ($S_F = l_c/l_f$);

In the equivalent FEMs the material features introduced are:

- E_m is the elastic modulus of the masonry;
- G_m is the shear modulus of the masonry;
- w_m is the specific weight of the masonry.

In particular, the sensitivity analyses are based on the influence of the geometrical slenderness of the perimeter walls and the slenderness of the façade. The slenderness of the perimeter walls and the façade change independently, keeping constant the height of both the walls and the façade and varying their thickness. At first, for each church, the geometrical slenderness of the perimeter walls changes while keeping constant all the other geometrical features. Then, the slenderness of the façade changes while keeping constant all the other geometrical features including the slenderness of the perimeter walls. Clearly, by varying the slenderness of the façade, different shape factors for each church are defined as well. The variations of the seismic responses are finally presented as a function of the slenderness of the perimeter walls, slenderness of the façade, and shape factor, for the four considered CLT roof configurations and under the same seismic actions.

Fig. 4 geometrical dimensions considered for the comparative analyses



3.2 Case studies

Sensitivity nonlinear dynamic analyses are performed in terms of the main geometrical features (Fig. 4 and Table 1), by varying the β parameter in the range $0.1 \leq \beta \leq 1.5$, under the same seismic action, on four one nave historical churches strengthened by CLT panels having different thicknesses. The aim is to analyze the seismic response in relation to the hysteretic variable β (already discussed in Sect. 2) and to investigate, for different roof-diaphragm configurations, the role of the slenderness of the perimeter walls, the one of the façade, and the ratio between the length and the width of each church. The churches considered in this work are (Fig. 5): Chiesa di San Pietro (located in Felizzano, AL), Chiesa di San Pietro Celestino (located in Isernia, IS), Chiesa di Santa Maria del Parco (located in Bojano, CB) and Chiesa di San Lorenzo (located in Tigliole, AT).

The characteristics of the masonry come from experimental tests and refer also to the Italian design code (NTC 2018) and Table C8A.2.1 of its commentary (Circolare 7, 2009). The three CLT panel roof structure configurations (namely CLT_t where t stand for the thickness of the CLT panel in cm, in the following) are characterized by the same connectors typology, $\Phi 10$ mm diameter steel screws with stiffness $k_c = 6500$ N/mm (Sandhaas and van de Kuilen 2017). A representation of the CLT roof structure configurations is given in Fig. 6. By varying β in the analyses, optimal β can be detected and consequently, by adopting the previous Eqs. (7–11), the optimal k_{roof} can be estimated as well. The seismic actions are introduced through seven spectra compatible accelerograms (Iervolino et al. 2010a, 2011) selected with REXEL 3.5 software (Iervolino et al. 2010b). It is important to notice that the considered earthquakes are referred to L'Aquila (Italy) city for a return period of 475 years (NTC 2018; Totani et al. 2016).

3.3 Results and remarks

To check the influence of the connection characteristics on the behavior of the roof structure, different scenarios having different β are considered. The results of the analyses with β varying in the range $0.1 \leq \beta \leq 1.5$ are given in terms of two dimensionless parameters: (i) displacement ratio (evaluated as the ratio between the lateral displacement of the central part of the roof and the target displacement chosen as the 0.5% of

Table 1 geometrical and materials features of the churches

Church	C	l_c [m]	l_f [m]	t_w [m]	h_w [m]	λ_w [-]	λ_f [-]	S_F [-]	E_m [MPa]	G_m [MPa]	w_m [kN/m ³]
San Pietro Felizzano	7	25	8.50	1.35	10.70	7.92	1.25	2.94	1500	500	18
San Pietro Celestino	4	24	8.75	1.50	11.10	7.40	1.26	2.74	1230	410	20
Santa Maria del Parco	6	33	10.00	1.50	11.75	9.79	1.18	3.30	1080	360	16
San Lorenzo	3	16	4.80	1.65	5.00	7.14	1.04	3.33	1050	350	18

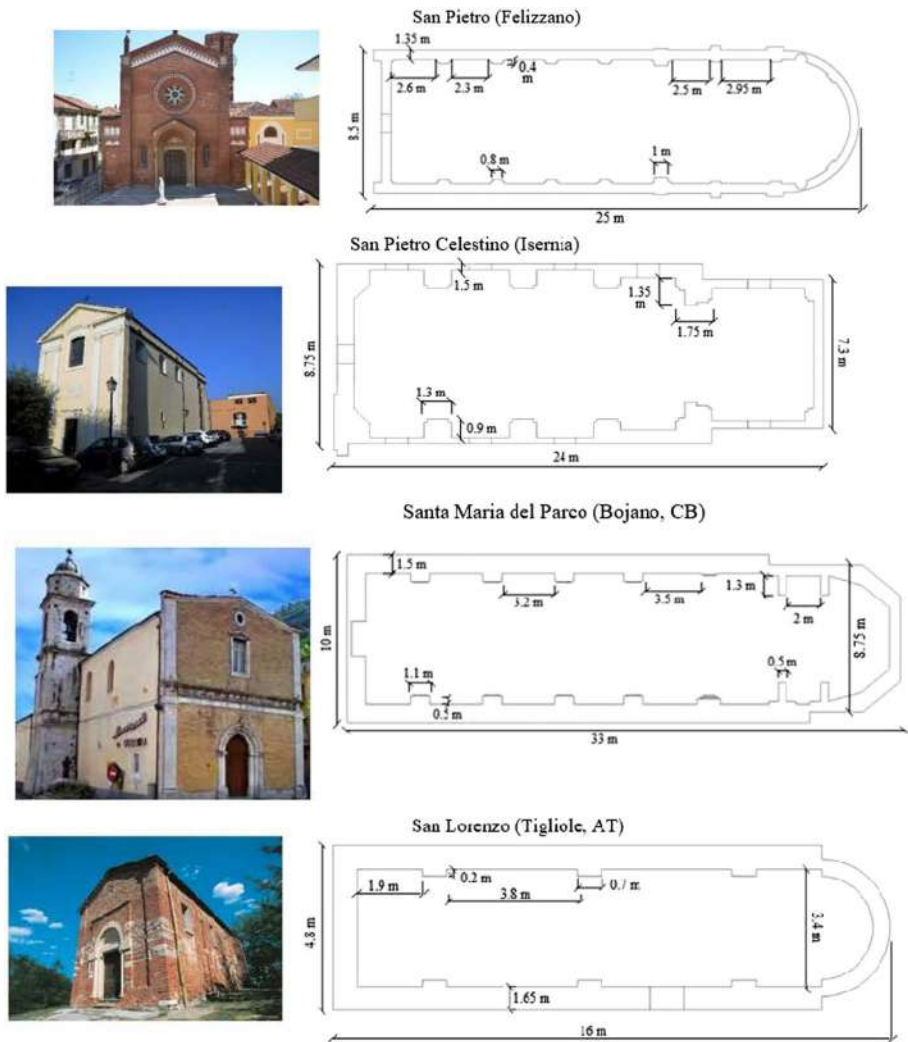


Fig. 5 the four churches under study

the height of the perimeter walls, according to the recommendation of the design code) and (ii) the force ratio (evaluated as the ratio between the base shear and the axial force on the façade). As discussed in paragraph 3.1, the considered parameters are: the geometrical slenderness of the walls ($\lambda_w = h_w/t_w$), the geometrical slenderness of the façade ($\lambda_f = h_f/l_f$) and the shape factor ($S_F = l_c/l_f$). By the equivalent finite element models of the churches, lateral displacements, base shear, and axial force are evaluated as the average values of the maximum ones, under the seven-spectrum compatible accelerograms. As an example of the displacement values obtained with the seven accelerograms, the average and standard deviation values for San Pietro Felizzano and San Lorenzo churches in one roof-configuration, already presented in paragraph 3.2 (CLT with $t = 6$ cm), are shown in Table 2. Moreover, for the same two churches, some results related to the plasticization of the inelastic hinges are provided too, for one of

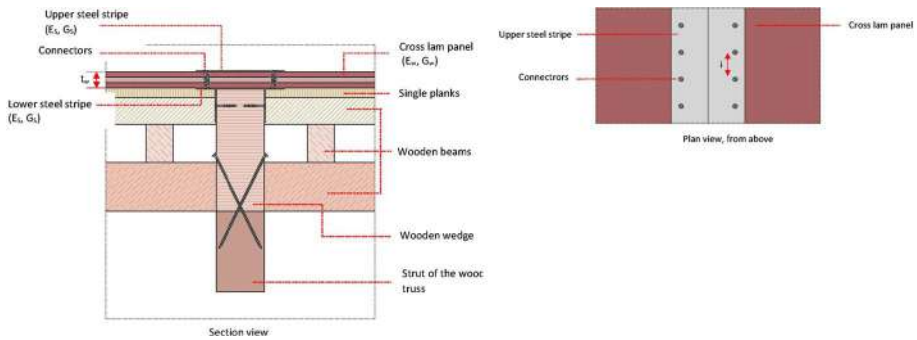


Fig. 6 CLT panels roof-structure configurations (example for three layers CLT panel)

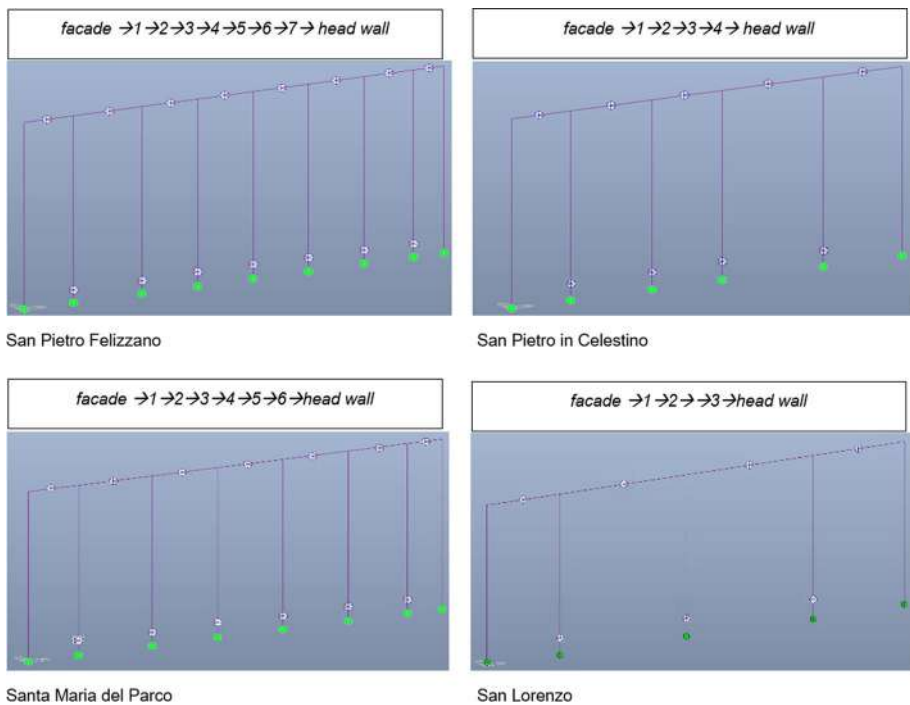


Fig. 7 EQ_FEM of the case studies

the seven spectrum-compatible accelerograms (S1), in order to detect the influence of the β values on their activation (Fig. 7).

The sensitivity analyses are performed as described in Sect. 3.1 and a possible optimized value of β can be determined, giving the possibility to design the corresponding characteristics of the connection with the Eqs. (3, 7, 12).

- (1) For β

Table 2 Geometrical slenderness of the perimeter walls: original dimensions and variations used in sensitivity analyses keeping constant the other geometrical features of the churches

	San Pietro Felizzano				San Pietro Celestino			
	Original	Variant 1	Variant 2	Variant 3	Original	Variant 1	Variant 2	Variant 3
t_w [m]	1.35	1.20	1.55	1.75	1.50	1.30	1.70	1.90
h_w [m]	10.70	10.70	10.70	10.70	11.10	11.10	11.10	11.10
λ_w	7.92	8.82	6.90	6.11	7.40	8.53	6.52	5.84
	San Lorenzo				San Maria del Parco			
	Original	Variant 1	Variant 2	Variant 3	Original	Variant 1	Variant 2	Variant 3
t_w [m]	0.70	0.60	0.90	1.10	1.20	1.05	1.35	1.50
h_w [m]	5.00	5.00	5.00	5.00	11.75	11.75	11.75	11.75
λ_w	7.14	8.33	5.55	4.54	9.79	11.19	8.70	7.83

The first investigation regards the detection of the optimum β value for each church with different roof diaphragm configurations (Fig. 8). In this investigation, the design displacement is assumed as the 0.5% of the perimeter walls height (the target displacements vary for each church in relation to the height of the perimeter walls, see also Table 1). It is worth nothing that the over resistant roof solution is not very influenced by the hysteretic variable β both for displacements and force ratios, giving low values of displacement ratio but very high values of the force ratio in comparison to the ones obtained from the CLT roof configurations.

From Figs. 8 and 9 it can be underlined that:

- A funding declaration is mandatory for publication in this journal. Please confirm that this declaration is accurate, or provide an alternative.
- the displacement ratio decreases for high β values because higher energy dissipation occurs in the roof-diaphragm according to Fig. 3;
- the force ratio is in opposition with respect to the displacement ratio;
- in case of an over stiffness solution, excessive values of force ratio are evaluated. This means possible incompatible in-plane shear actions with respect to the geometry and material properties of the façades;
- the effectiveness of the over stiffness solution is especially compromised in terms of force ratio: the case studies show values almost doubled of the dissipative configurations.

The second investigation regards the percentage variation of lateral displacements ($\Delta\eta$), for each church, with the three CLT solutions by changing β with respect to the unreinforced wooden roof-structure with 4 cm single-layer planks. The trends shown in Fig. 10 are useful to understand the improvements of the seismic responses with increasing β .

From Fig. 10 it can be highlighted that:

- for the same church, the variations are more evident for panels with higher thickness.
- in correspondence of $\beta = 1.5$, the variations are around 50% in average for each church with 100 mm thickness panels.

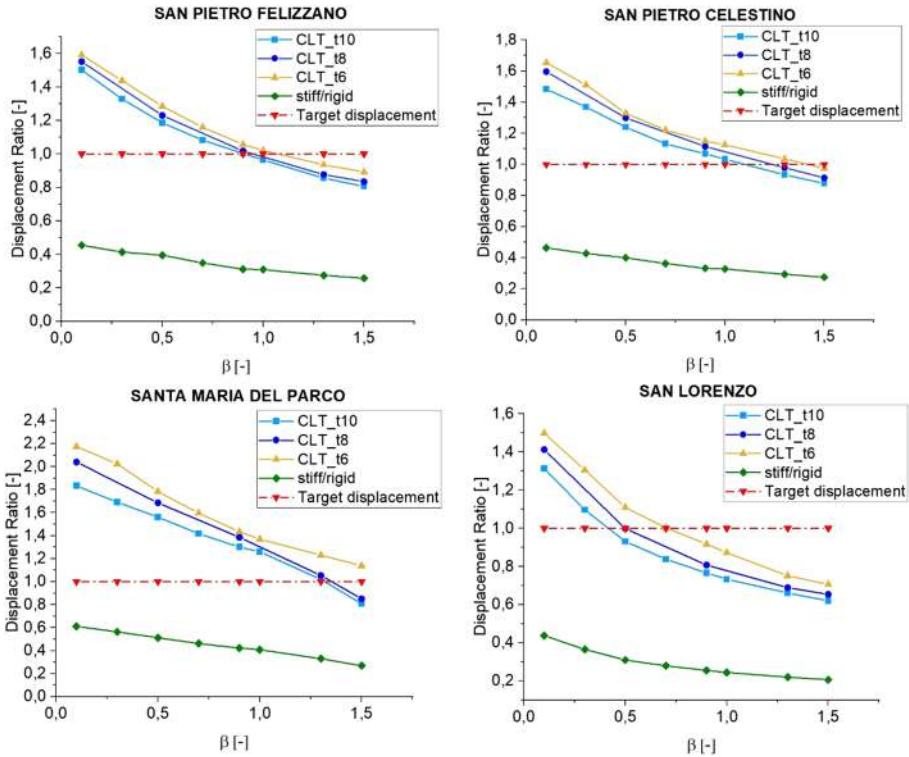


Fig. 8 Displacement ratio (lateral displacement/target displacement) as a function of β

The third investigation regards the differential rocking of the piers by detecting the transverse displacements of the roof's nodes and the mutual distance between the equivalent vertical elements (measured from the façade). For the sake of brevity, this supplementary analysis is carried out for the CLT roof configuration having 6 cm thickness. From the equivalent models, analyzed under the seven-spectrum compatible accelerograms, it can be observed that the central nodes of the roof show the highest lateral displacements, whereas the top nodes of the façade and head wall have displacements close to zero. For a church, by varying β , the displacements of roof's nodes are calculated under the seismic actions and the average values are detected as well. Consequently, for different β -values, the ratios between the average top displacement and the height of the perimeter walls are evaluated in percentage terms. In this way, the rocking can be plotted in terms of the story drift ratio versus the mutual distances between the vertical equivalent elements. In Fig. 11, the different rocking of the case studies are shown for the CLT roof configuration with 6 cm thickness.

From Fig. 11, the following conclusions can be drawn:

- the transverse deformed shape of the roof depends on the mutual distance of the vertical equivalent elements;

- the corresponding deformed shapes for other thicknesses (8 and 10 cm) are similar but the story-drift ratios are lower than the ones plotted for the 6 cm thickness configuration;
- the flattening of the curve is more evident passing from $\beta=0.1$ to $\beta=0.9$. For higher β values, close to the limit value $\beta=1.5$, the story drift ratio changes are significantly less evident.

The fourth investigation regards the influence of β on the activation of the inelastic hinges of both the equivalent walls and roof elements. As it was mentioned in the previous Sect. 2.1, (i) the equivalent walls have concentrated inelastic rotational springs at their base, described by a trilinear $M-\chi$ model (the behavior of these hinges is represented in Fig. 12, referred as R_y), (ii) the nonlinear behavior of the roofing system is represented by means of inelastic shear sliders described by a hysteretic Clough model (the behavior of these sliders is reported in Fig. 12, denoted with D_y). For the sake of brevity, the presented results concern only San Pietro Felizzano and San Lorenzo churches, already taken as an example in Sect. 3.2, under the spectrum compatible accelerogram S1. In Fig. 12, the symbol 1 (blue) represents the plastic hinges remaining in the elastic field, whereas the symbol 2 (green) represents the activated plastic hinges.

From Fig. 12, it can be noticed that:

- by increasing β , the number of activated inelastic hinges on the roof decreases. Generally, the hinges located at both ends of the roof are always activated, contributing to dissipation of energy, whereas the central part of the roof shows an increasing number of hinges remaining in the elastic field;
- the number of activated plastic hinges of the walls increases for β ranging from 0.1 to 0.9 while, beyond 0.9, the number of inelastic hinges actually dissipating energy decreases.

(2) The influence of the walls' slenderness (λ_w)

The influence of the geometrical slenderness of the perimeter walls λ_w on the seismic response in terms of displacements ratio is analyzed focusing on the results obtained for the central equivalent element of each finite element model. The central element is located in correspondence of the roof's part afflicted by the maximum lateral displacement. Moreover, the influence of the geometrical slenderness of the perimeter walls λ_w on the seismic response in terms of force ratio is also analyzed focusing on the results obtained for the equivalent element representing the façade, in each finite element model. The role of λ_w is here investigated for 6, 8, and 10 cm panel thickness by varying β in the range $0.1 \leq \beta \leq 1.5$. The slenderness considered are shown in Table 3.

From Figs. 13, 14, 15, 16, the following considerations can be drawn:

- (3) the lateral displacements increase with geometrical slenderness of the perimeter walls;
- (4) the geometrical slenderness of the perimeter walls influences the seismic response in terms of displacements particularly in the range $4.5 \leq \lambda_w \leq 9$;
- (5) beyond $\lambda_w \approx 9$, the variation of the geometrical slenderness slightly afflicts the seismic response in terms of displacements, as it is for Santa Maria del Parco church;
- (6) in the range $4.5 \leq \lambda_w \leq 9$, the variation in terms of displacements is about 50% in average; by increasing the slenderness of the perimeter walls beyond $\lambda_w \approx 9$ up to (about) 11.50, the variation is about 17%.
- (7) the hysteretic variable β influences the lateral displacements for the same CLT roof configuration. The most evident variation is present passing from $\beta=0.1$ to $\beta=0.5$,

Fig. 9 force ratio (base shear/axial force on the façade) as a function of β : (left) the diagrams of the CLT roof—diaphragm in comparison to the over stiff/rigid roof solution, (right) the diagrams related only to the CLT roof—diaphragm configurations

while from $\beta = 0.9$ to $\beta = 1.5$ the curves of the diagrams are closer, especially for San Pietro Felizzano, San Pietro Celestino and San Lorenzo churches;

- (8) for the same panel thickness and the same slenderness of the perimeter walls, the spacing of the connectors (for the same screw diameter and cross section of the steel stripes) seems slightly afflict the lateral displacements because the seismic response seems much more depending on the panel thickness.
- (9) The influence of the slenderness of the façade (λ_f).

The influence of the geometrical slenderness of the façade λ_f in the nave transversal response in terms of displacements ratio is analyzed focusing on the results found for the central equivalent element of each finite element model. Moreover, the influence of λ_f in terms of force ratio is analyzed focusing on the results detected for the façade element, for the various models. The role of the slenderness is here investigated for 6, 8, and 10 cm panel thicknesses by changing β in the range $0.1 \leq \beta \leq 1.5$. The slenderness values of the façade are shown in Table 4.

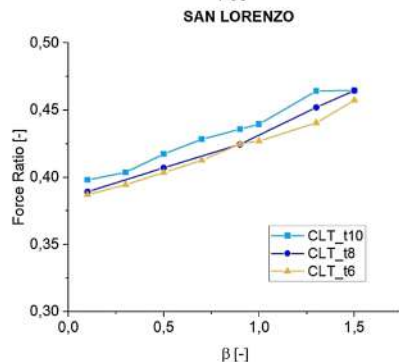
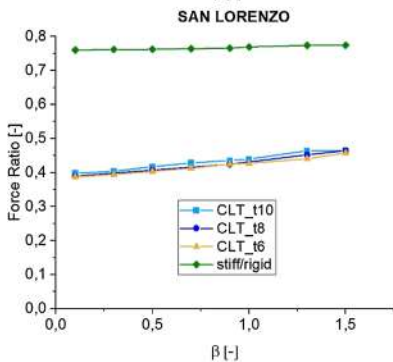
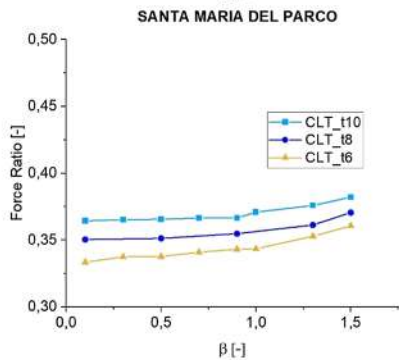
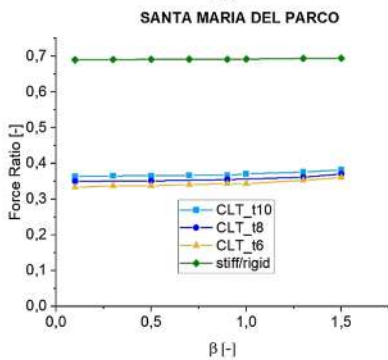
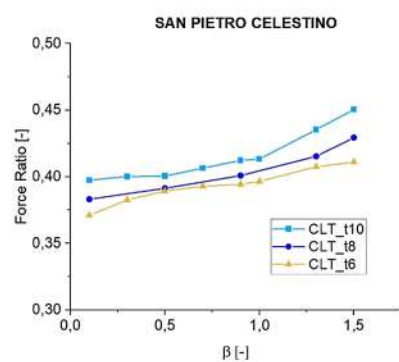
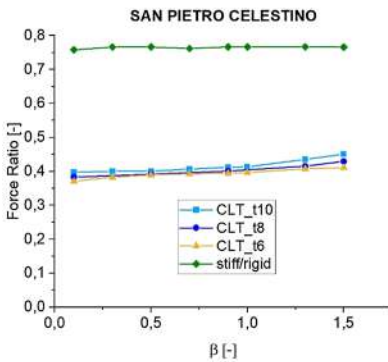
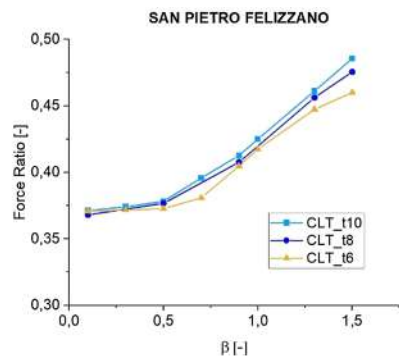
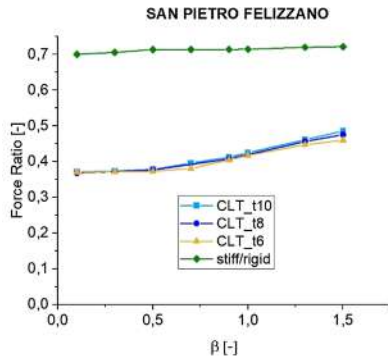
From Figs. 17, 18, 19, 20, the following considerations can be highlighted:

- (10) the lateral displacements are less influenced by the geometrical slenderness of the façade λ_f with respect to the slenderness of the perimeter walls λ_w . Nevertheless, when the slenderness of the façade increases, keeping constant the geometry of the perimeter walls, the lateral displacements increase as well;
- (11) in the wide range $0.9 \leq \lambda_f \leq 1.9$, the variations in terms of displacements are about 18% in average;
- (12) for the same slenderness of the façade, the same diameter of the connectors, and the same cross section of the steel stripes, the response is much more influenced by the CLT panel thickness than the spacing of the connections.
- (13) The influence of the shape factor (S_f).

The influence of the shape factor (defined as the ratio between the length and the width of the church) in the nave transversal response in terms of displacement ratio is analyzed focusing on the results obtained for the central equivalent element of each finite element model. The role of the shape factor is here investigated for the three roof diaphragm configurations (previous Table 5) by varying β in the range $0.1 \leq \beta \leq 1.5$. The slenderness of the façade here considered are shown in Table 5.

From Figs. 21, 22, 23, 24, the following considerations can be observed:

- (14) the shape factor S_f influences the seismic response under transversal earthquake either in terms of displacements or shear on the façade; the trends referring to the lateral displacements are opposite with respect to the ones related to the shear on the façade;
- (15) the lateral displacements are less influenced by the shape factor S_f with respect to the slenderness of the perimeter walls. The trends are similar to the ones obtained by varying the slenderness of the façade λ_f . Nevertheless, when the shape factor increases, keeping constant the geometry of the perimeter walls, the lateral displacements tendentially increases as well;
- (16) in the wide range $2.10 \leq S_f \leq 4.00$ the variations in terms of displacements are about 15% in average;
- (17) the hysteretic variable β influences the lateral displacements for the same CLT roof structural configuration; the most evident variation is present passing from $\beta = 0.1$



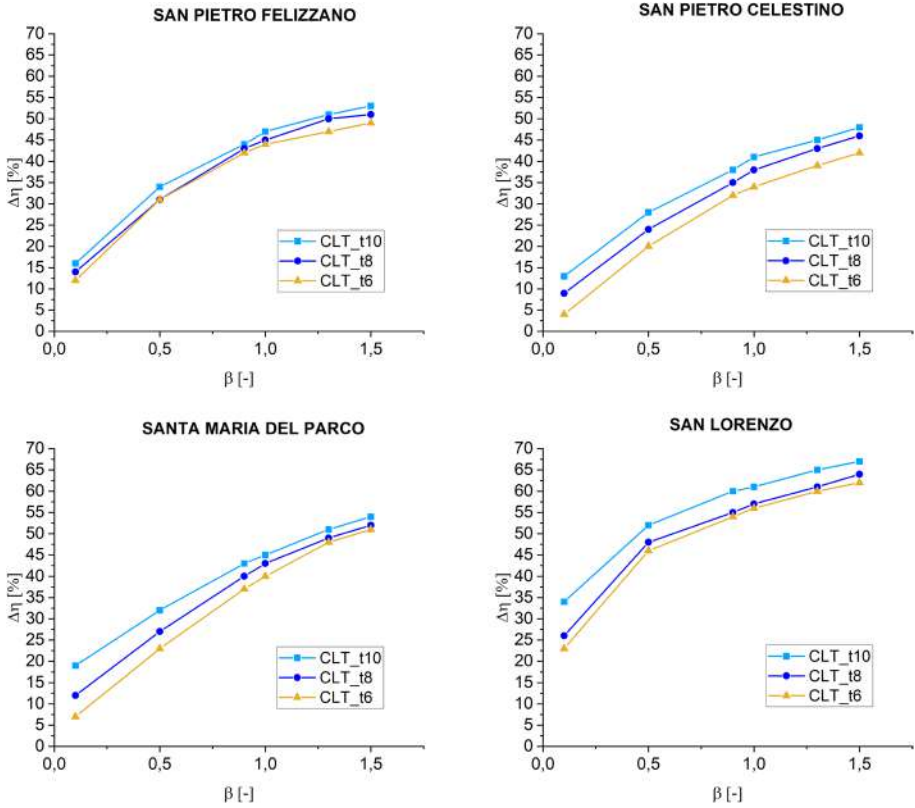


Fig. 10 percentage variation $\Delta\eta$ [%] of lateral displacements between unreinforced wooden roof structure characterized by 4 cm single-layer planks and the three CLT roof- diaphragm proposed configurations

to $\beta=0.5$; from $\beta=0.9$ to $\beta=1.5$ the curves of the diagrams are closer for all the churches here analyzed.

4 Conclusions

In the present work, the influence of the geometrical features on the nave transversal response of four historical masonry churches, strengthened with different CLT panel roof structures, is deepened by nonlinear dynamic analyses. The seismic analyses have been performed by equivalent finite element models with concentrated nonlinear properties of the masonry walls and the roof-diaphragm, under the transversal seismic input represented by seven spectrum compatible accelerograms. In such analyses, the effectiveness of the proposed CLT strengthening technique is appreciable both in terms of lateral displacements and shear action on the façade.

The followings remarks can be stated:

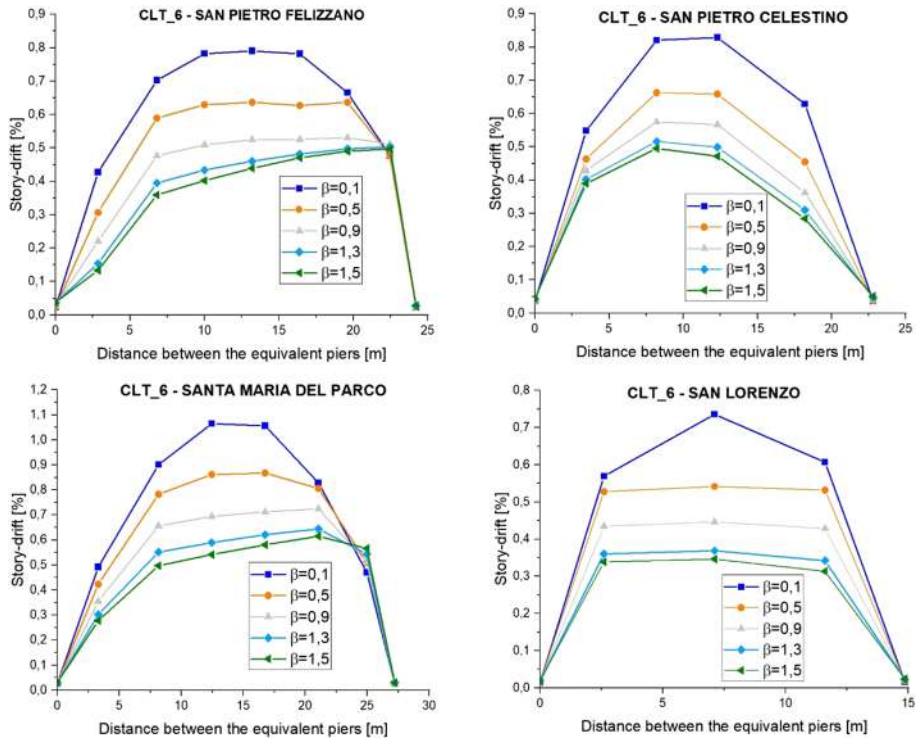
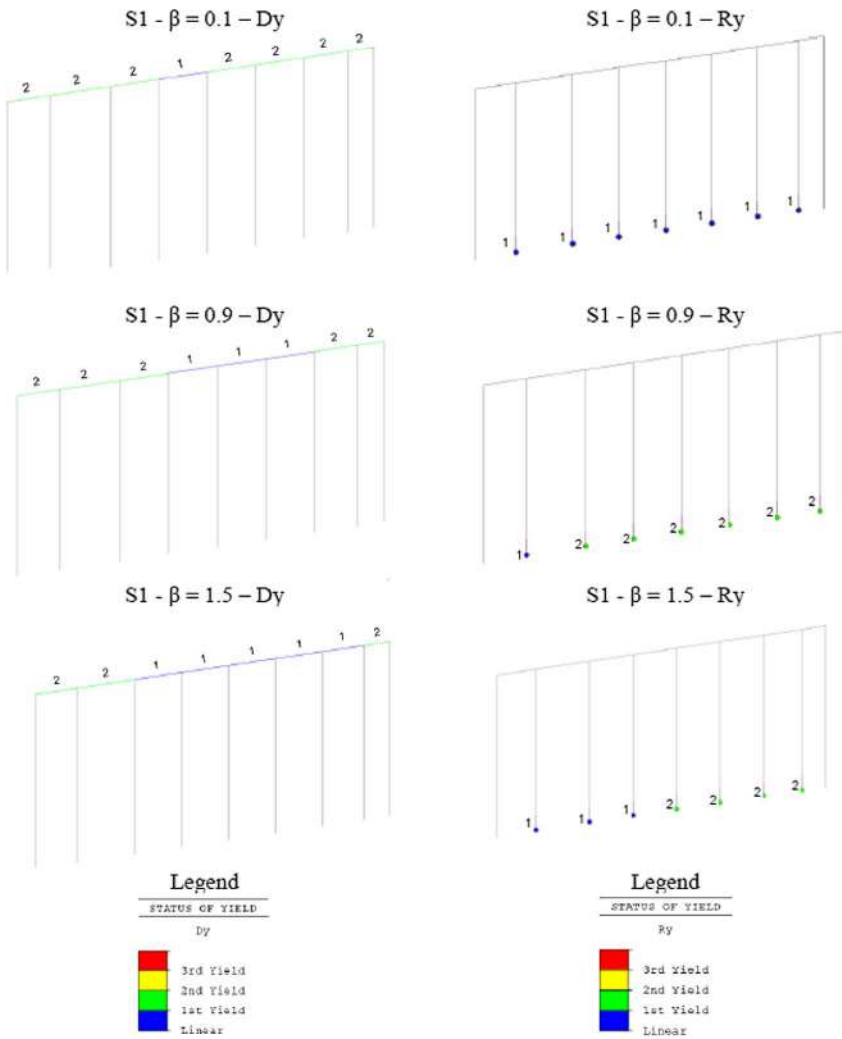


Fig. 11 differential rocking with CLT (thickness $t=6$ cm) roof structure

- in seismic restoration of historical churches, the CLT panel roof-structure can be considered as a valid solution both for the structural benefits in the nave transversal response and the satisfaction of the heritage conservation criteria;
- the equivalent finite element model with concentrated nonlinear plastic hinges (for both the masonry and the roof-diaphragm) allows to evaluate the global response of historical churches with a low calculation cost;
- the damped rocking mechanism pursued by CLT panel dissipative roof-structure is mainly ruled by the variation of the hysteretic variable β that gives a measure of the energy dissipation; the calibration of β is preferable in the range $0.1 \leq \beta \leq 1.5$ in order to limit the transversal top displacement under the design recommended value, guaranteeing the self-centering rocking behavior and limiting the actions on the head and perimeter walls;
- the displacement trends detected by nonlinear dynamic analyses are opposite to those of the shear. The proposed roofing system, through its dissipating behavior controlled by the plasticization of the connections, has the capacity to limit the shear transfer to the façade/head wall when the connections yield and the top displacements of the central spans increases;
- the displacement and base shear variations depend on the thickness of the CLT panel, based on the stiffness of the roof;
- the thickness of the CLT panels seems to not afflict significantly the influence of the perimeter walls slenderness on the seismic response, in terms of displacements and

SAN PIETRO FELIZZANO



(a)

SAN LORENZO

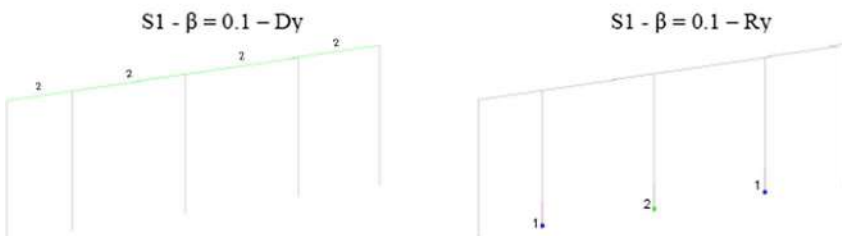


Fig. 12 indication of the yielding status of the inelastic hinges of San Pietro Felizzano (a) and San Lorenzo (b) churches, under the accelerogram S1 for different β values

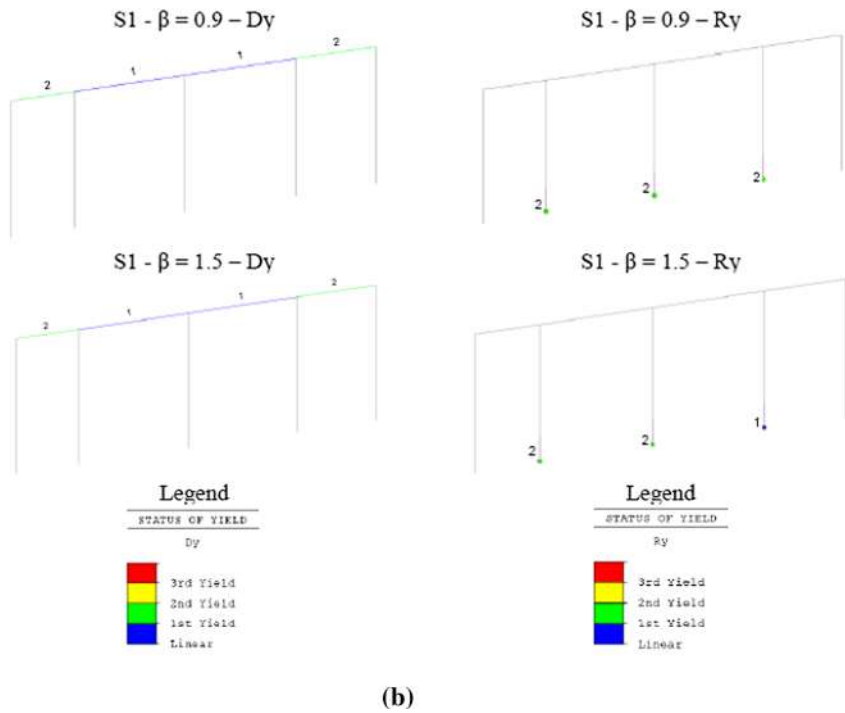


Fig. 12 (continued)

Table 3 Geometrical slenderness of the façade: original dimensions and variations used in sensibility analyses, keeping constant the other geometrical features of the churches

	San Pietro Felizzano				San Pietro Celestino			
	Original	Variant 1	Variant 2	Variant 3	Original	Variant 1	Variant 2	Variant 3
l_f [m]	8.50	7.50	10.00	11.50	8.75	7.00	9.50	10.50
λ_f	1.25	1.62	1.21	1.05	1.26	1.87	1.38	1.25
	San Lorenzo				San Maria del Parco			
	Original	Variant 1	Variant 2	Variant 3	Original	Variant 1	Variant 2	Variant 3
l_f [m]	4.80	4.00	6.00	7.00	10.00	8.50	11.50	13.00
λ_f	1.35	1.62	1.08	0.93	1.27	1.50	1.10	0.98

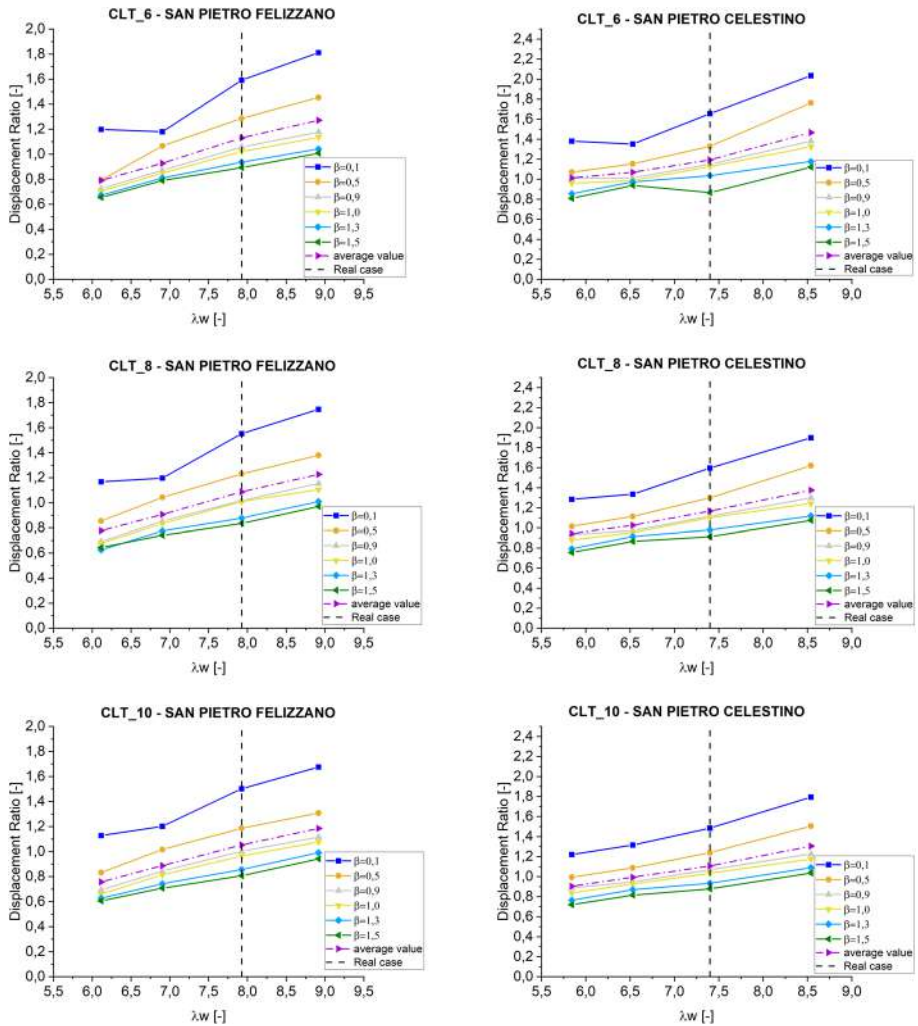


Fig. 13 displacement ratio (lateral displacement/target displacement) for San Pietro Felizzano and San Pietro Celestino in relation to the geometrical slenderness of the lateral walls (λw) for the three different CLT roof structure configurations

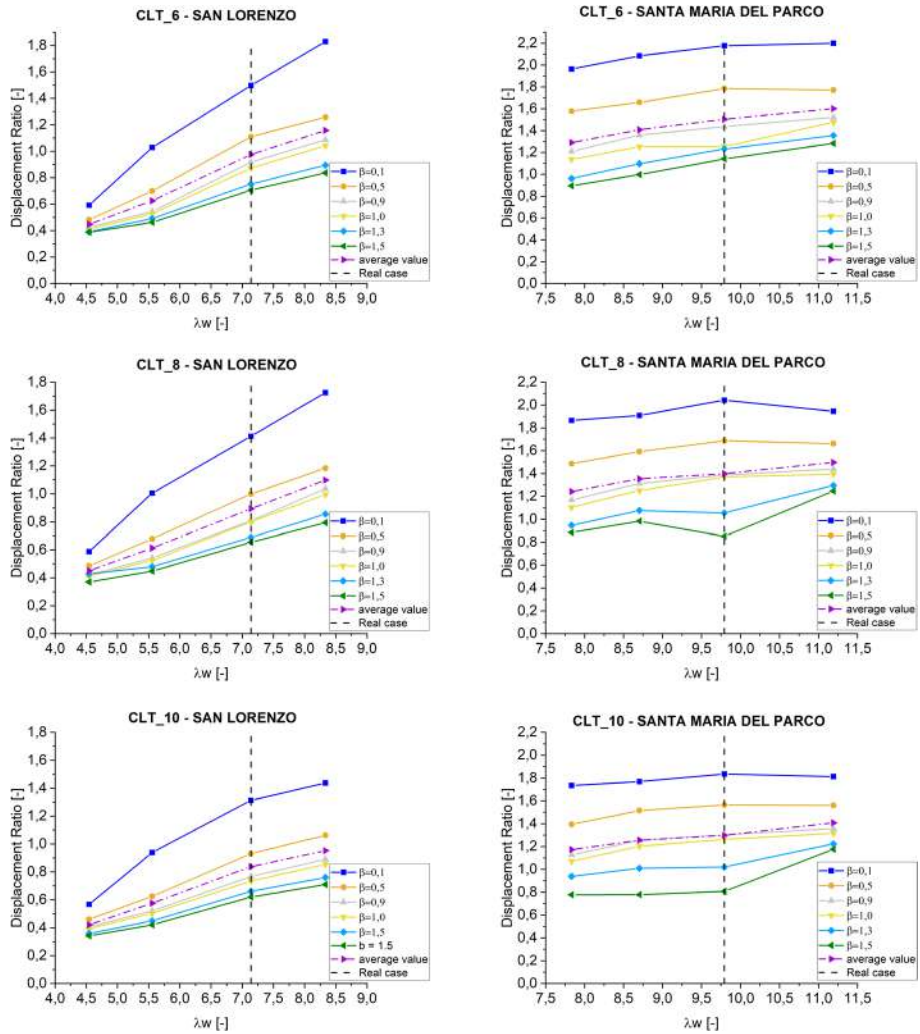


Fig. 14 displacement ratio (lateral displacement/target displacement) for San Lorenzo and Santa Maria del Parco in relation to the geometrical slenderness of the lateral walls (λw) for the three different CLT roof structure configurations

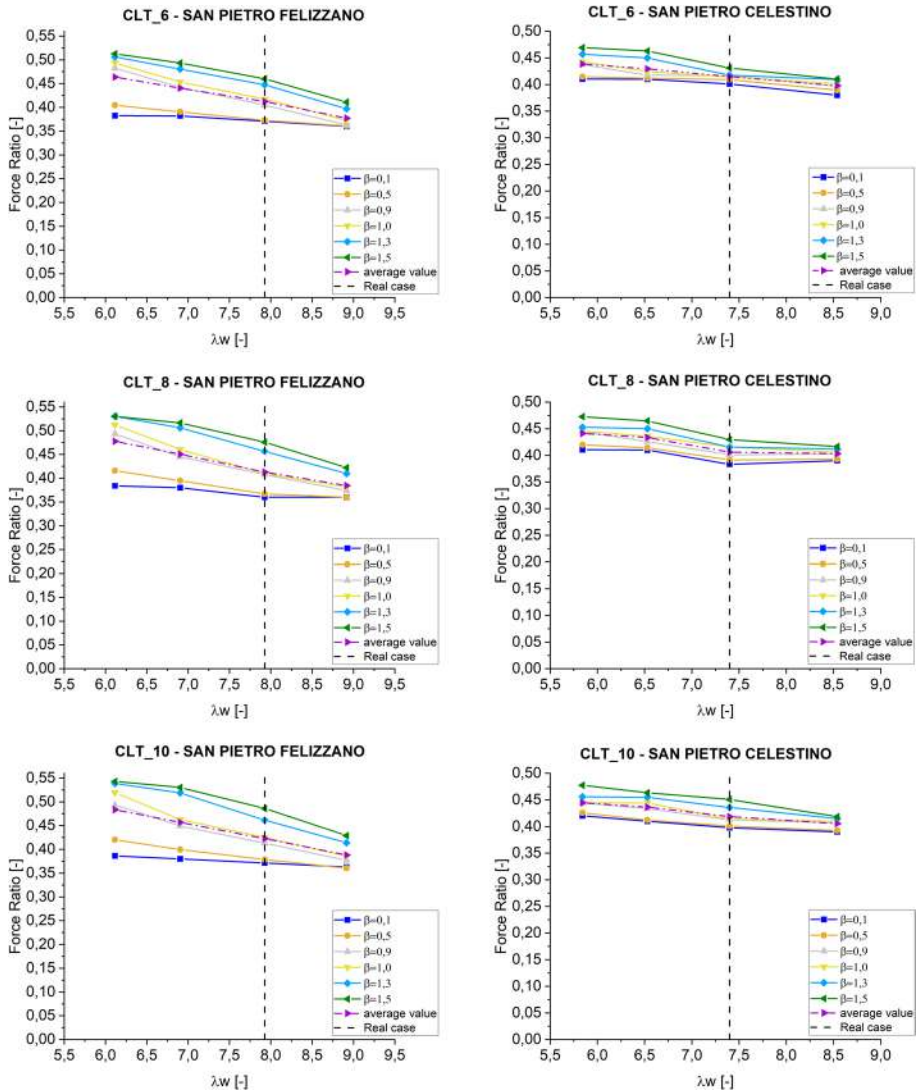


Fig. 15 force ratio (base shear/axial force on the facade) for San Pietro Felizzano and San Pietro San Pietro Celestino in relation to the geometrical slenderness of the lateral walls (λw) for the three different CLT roof structure configurations

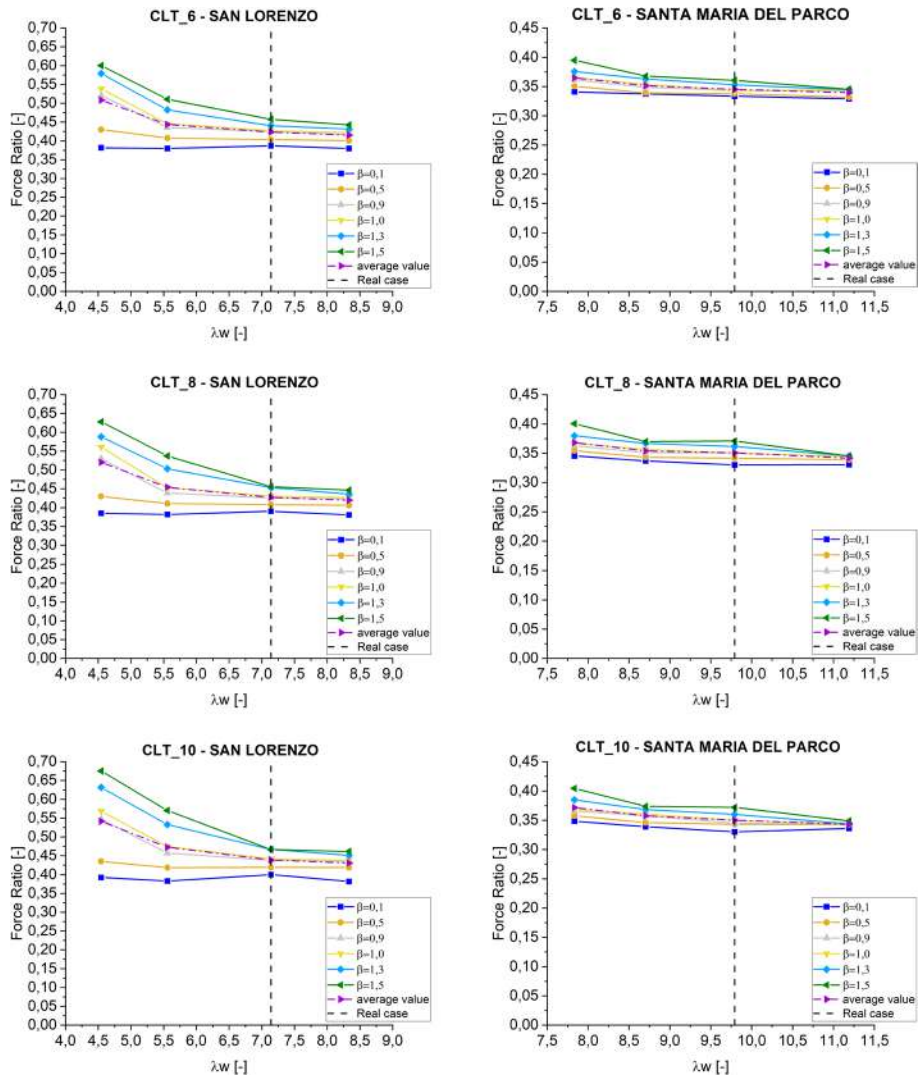


Fig. 16 force ratio (base shear/axial force on the facade) for San Lorenzo and Santa Maria del Parco in relation to the geometrical slenderness of the lateral walls (λw) for the three different CLT roof structure configurations

Table 4 Shape factors for the case studies: original values and variations

	San Pietro Felizzano				San Pietro Celestino			
	Original	Variant 1	Variant 2	Variant 3	Original	Variant 1	Variant 2	Variant 3
l_f [m]	8.50	7.50	10.00	11.50	8.75	7.00	9.50	10.50
l_c [m]	25	25	25	25	24	24	24	24
S_f	2.94	3.33	2.50	2.17	2.74	3.43	2.53	2.28
	San Lorenzo				San Maria del Parco			
	Original	Variant 1	Variant 2	Variant 3	Original	Variant 1	Variant 2	Variant 3
l_f [m]	4.80	4.00	6.00	7.00	10.00	8.50	11.50	13.00
l_c [m]	16	16	16	16	33	33	33	33
S_f	3.33	4.00	2.67	2.28	3.30	3.88	2.87	2.54

shear on the façade. Analogous statement can be formulated for the influence of the façade slenderness. In this kind of application, the range of possible considered CLT thicknesses is limited by construction limitations. This follows in a corresponding limited influence of the CLT thickness on the results, with respect to the other properties;

- in the nave transversal response, for greater values of the perimeter walls slenderness, the slenderness of the façade, and the shape factor, the displacement ratio increases while the force ratio decreases, as a result of the limitation of the shear actions in the roof caused by the plasticization of the connections;
- in the present cases studies, the geometrical slenderness of the façade λ_f (considering the range $1.05 \leq \lambda_f \leq 1.60$) influences the variation of the transversal response of the churches in terms of displacement ratio for about 18% in average and in terms of force ratio on the façade for about 6%. The influence of the geometrical slenderness of the perimeter walls seems more appreciable than the slenderness of the façade and the shape factor on the nave transversal response;
- the force ratio on the façade is lower for thinner CLT panels, in opposition to the displacement ratio. The calibration of the thickness of the panels in relation to the diameters and spacing of the connections is mandatory in order to guarantee, as far as possible, a global box behavior of the one nave church under transversal seismic actions.

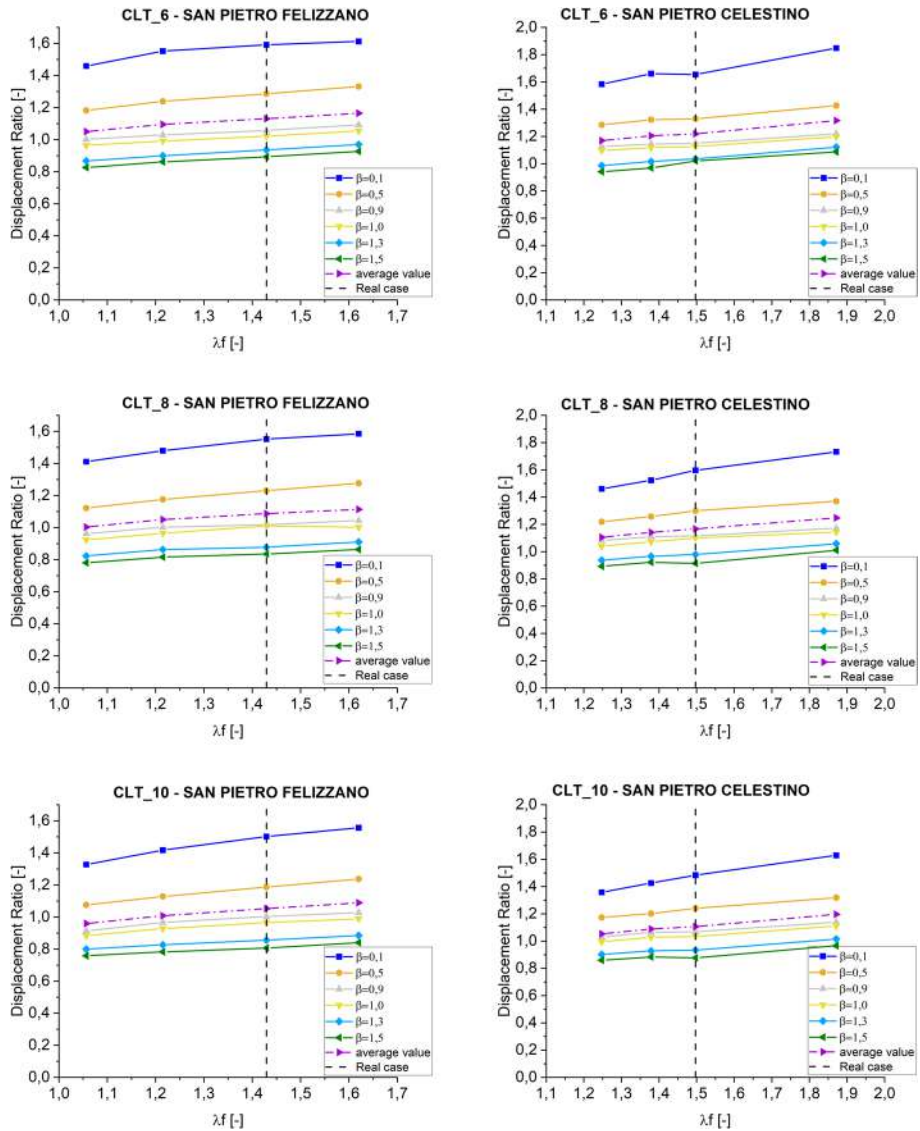


Fig. 17 displacement ratio (lateral displacement/target displacement) for San Pietro Felizzano and San Pietro Celestino as a function of the geometrical slenderness of the facade (λf) for three different CLT roof structure configurations

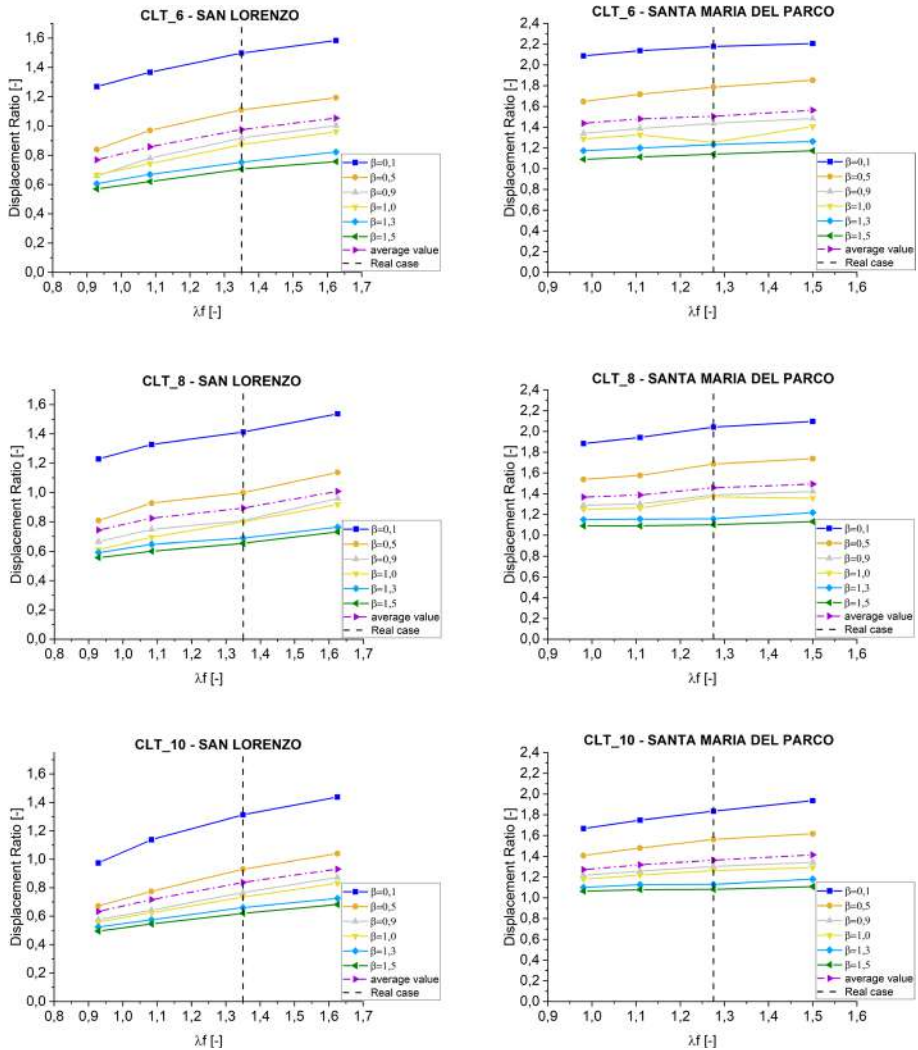


Fig. 18 displacement ratio (lateral displacement/target displacement) for San Lorenzo and Santa Maria del Parco as a function of the geometrical slenderness of the facade (λ_f) for three different CLT roof structure configurations

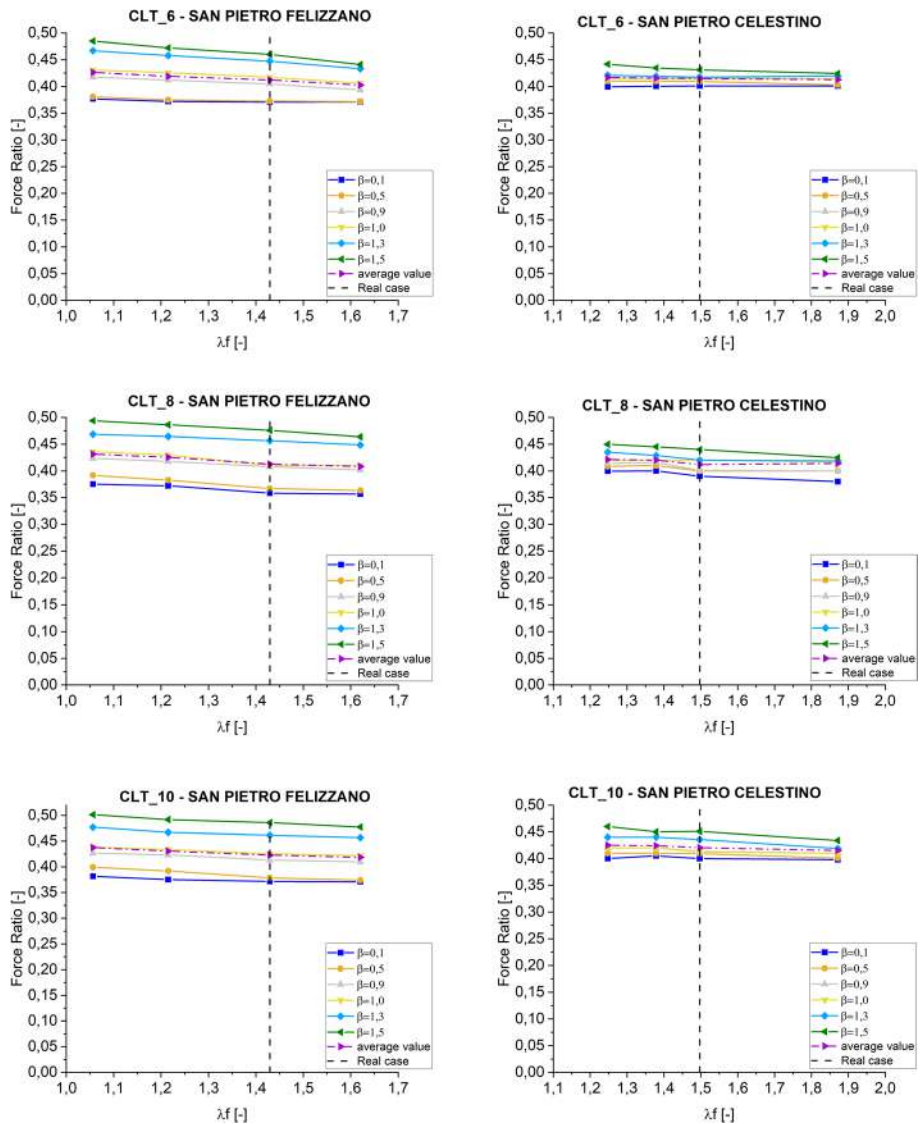


Fig. 19 force ratio (base shear/axial load on the façade) for San Pietro Felizzano and San Pietro Celestino as a function of the geometrical slenderness of the façade (λf) for three different CLT roof structure configurations

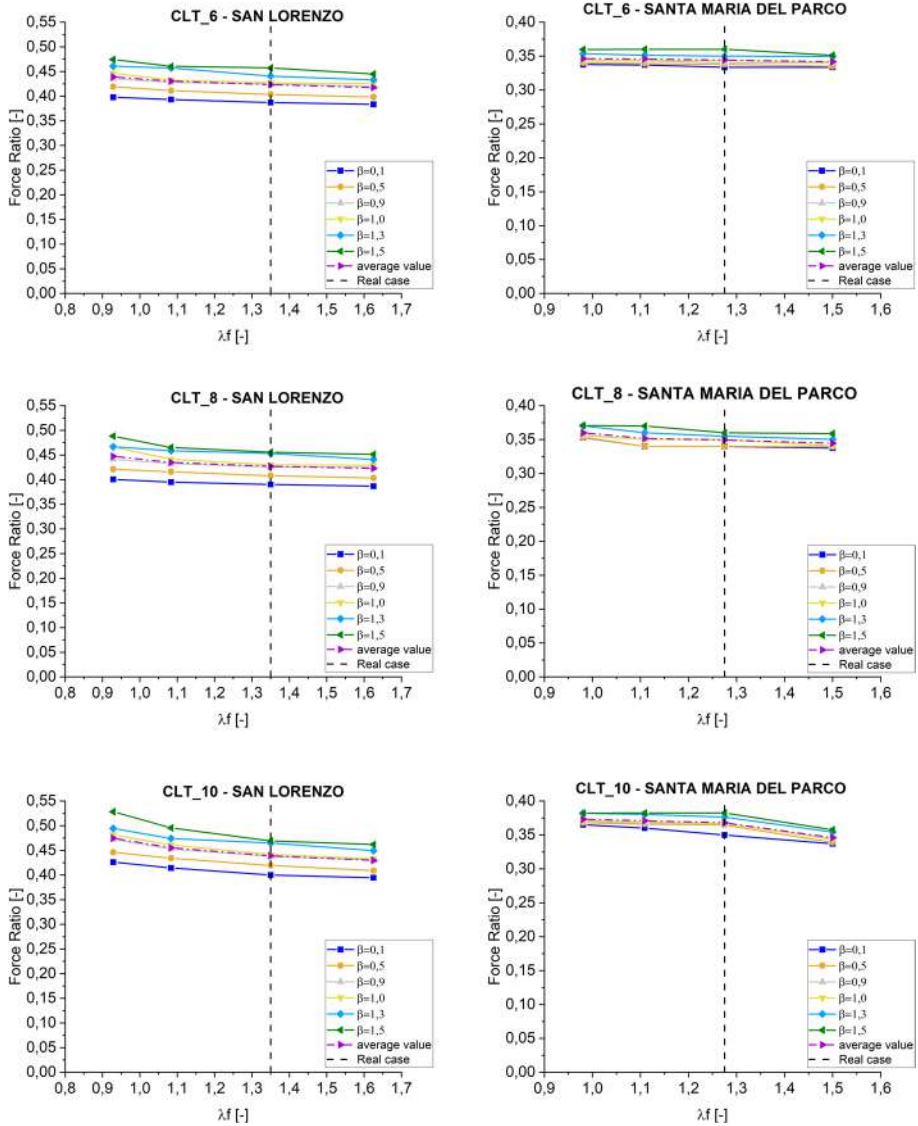


Fig. 20 Force ratio (base shear/axial load on the façade) for San Lorenzo and Santa Maria del Parco as a function of the geometrical slenderness of the façade (λf) for three different CLT roof structure configurations

Table 5 An example of the displacements for a CLT roof configuration under the seven-spectrum compatible accelerograms for San Pietro Felizzano and San Lorenzo churches

<i>San Pietro Felizzano—CLT=6 cm, displacements (absolute values) [m]</i>									
	Acc_1	Acc_2	Acc_3	Acc_4	Acc_5	Acc_6	Acc_7	average	stand.dev
$\beta=0.1$	0.110	0.085	0.072	0.062	0.110	0.074	0.081	0.085	0.019
$\beta=0.5$	0.074	0.066	0.054	0.049	0.088	0.071	0.076	0.068	0.013
$\beta=1.5$	0.046	0.053	0.040	0.047	0.056	0.043	0.047	0.047	0.005
<i>San Lorenzo—CLT=6 cm, displacements (absolute values) [m]</i>									
	Acc_1	Acc_2	Acc_3	Acc_4	Acc_5	Acc_6	Acc_7	average	stand.dev
$\beta=0.1$	0.057	0.045	0.028	0.040	0.027	0.028	0.038	0.040	0.011
$\beta=0.5$	0.036	0.036	0.022	0.027	0.022	0.022	0.025	0.027	0.006
$\beta=1.5$	0.020	0.020	0.017	0.016	0.014	0.018	0.015	0.017	0.002

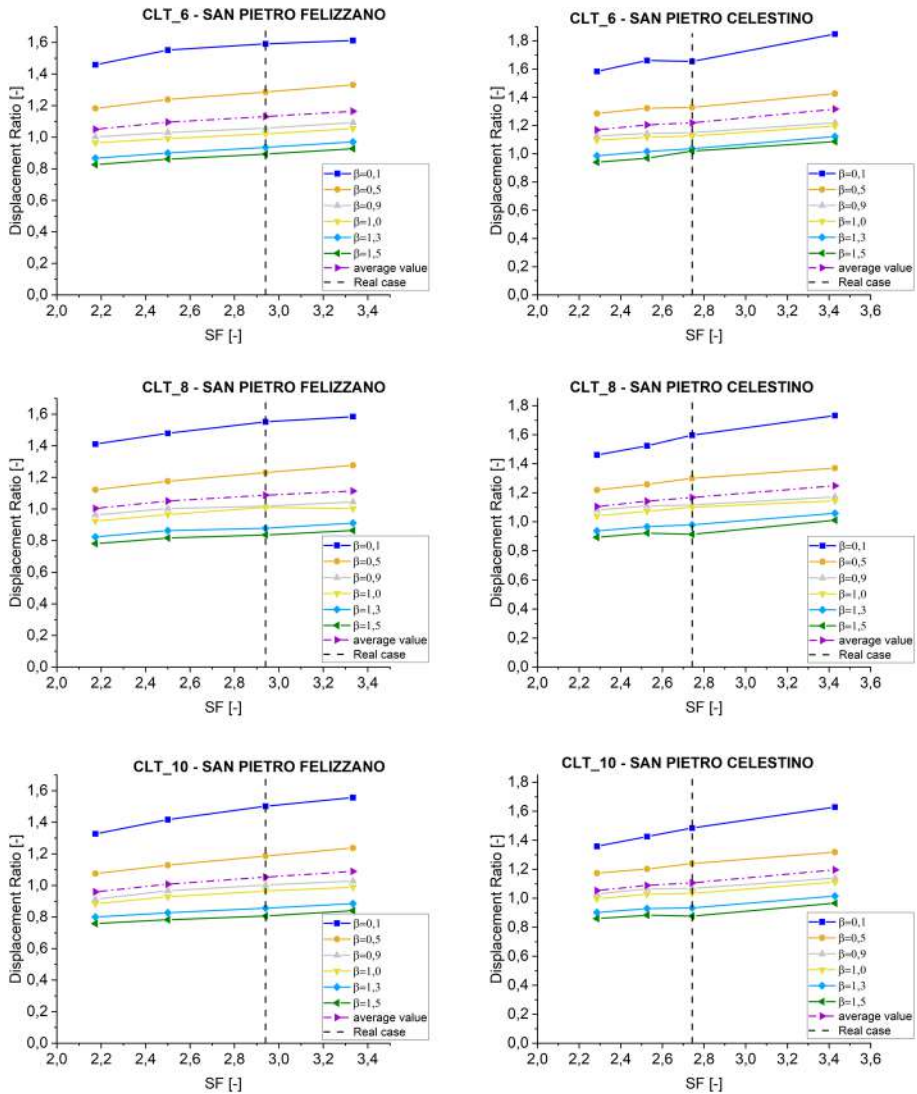


Fig. 21 Displacement ratio (lateral displacement/target displacement) for San Pietro Felizzano and San Pietro Celestino in relation to the shape factor (Sf) for three different CLT roof structure configurations

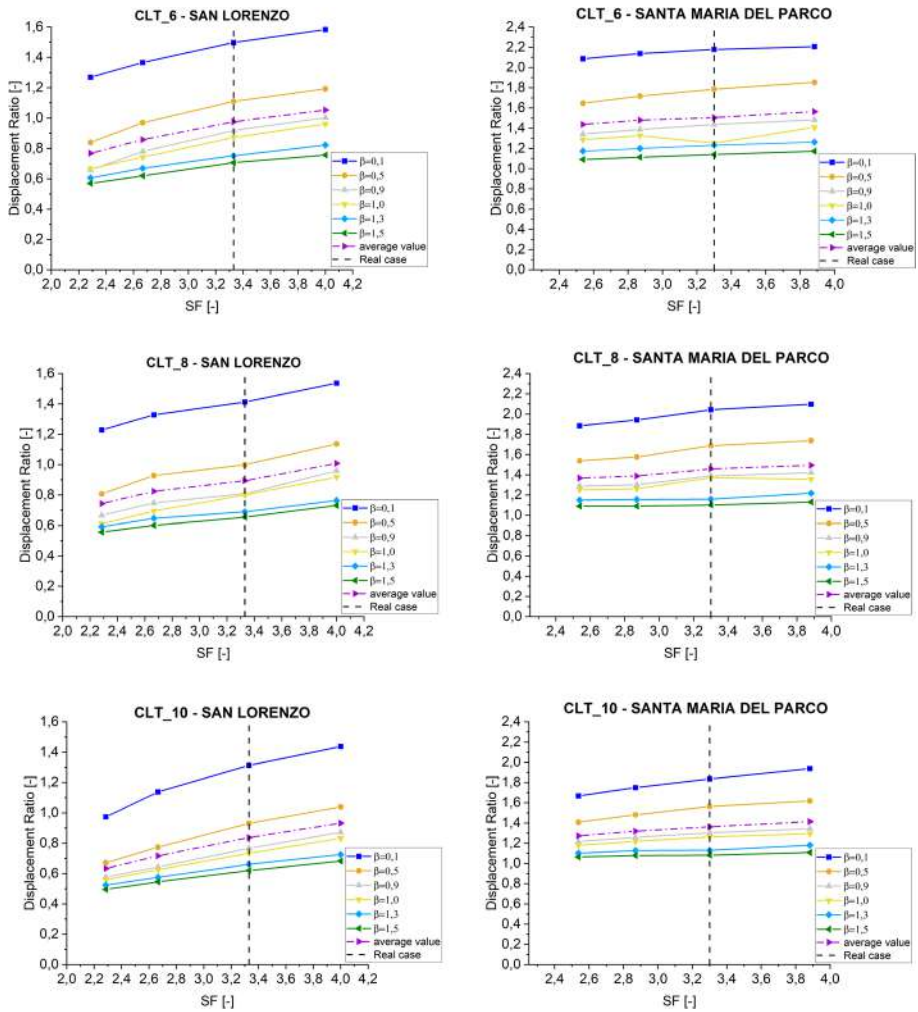


Fig. 22 Displacement ratio (lateral displacement/target displacement) for San Lorenzo and Santa Maria del Parco in relation to the shape factor (Sf) for three different CLT roof structure configurations

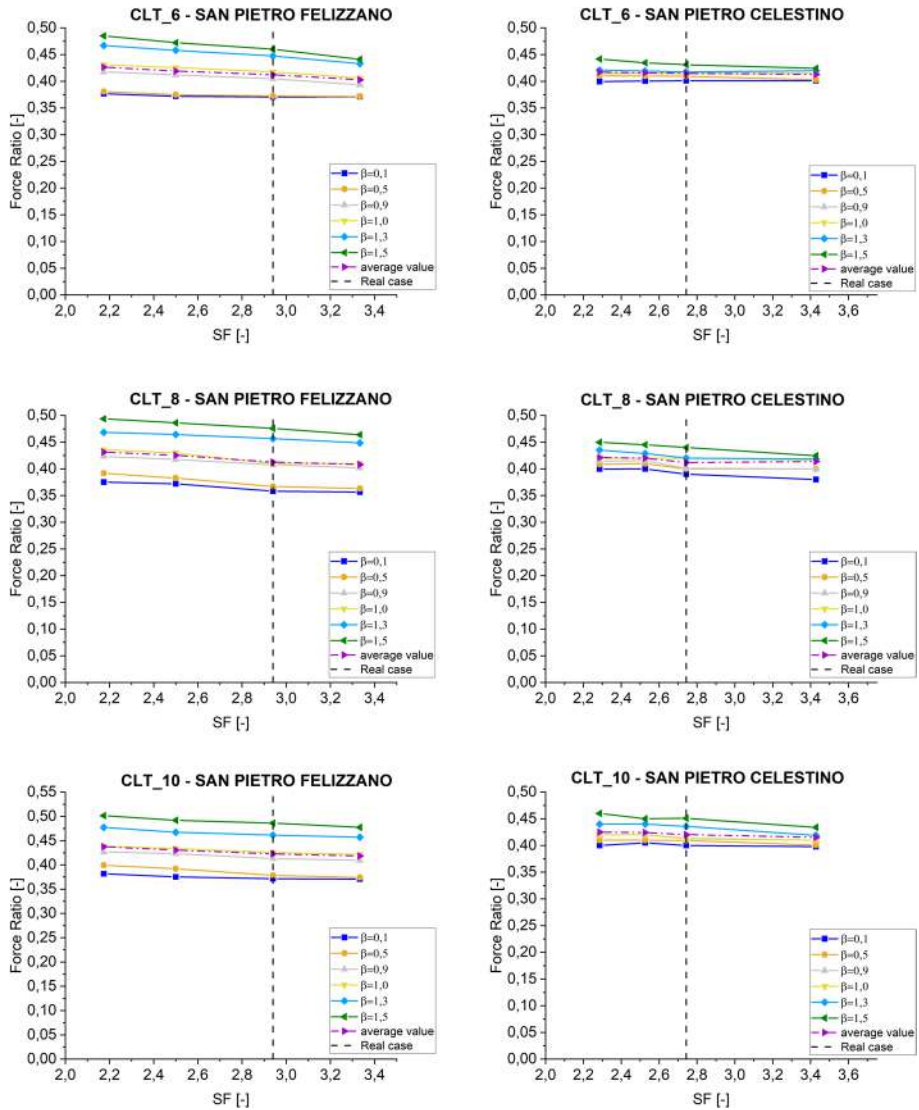


Fig. 23 Force ratio (base shear/axial load on the façade) for San Pietro Felizzano and San Pietro Celestino in relation to the shape factor (Sf) for three different CLT roof structure configurations

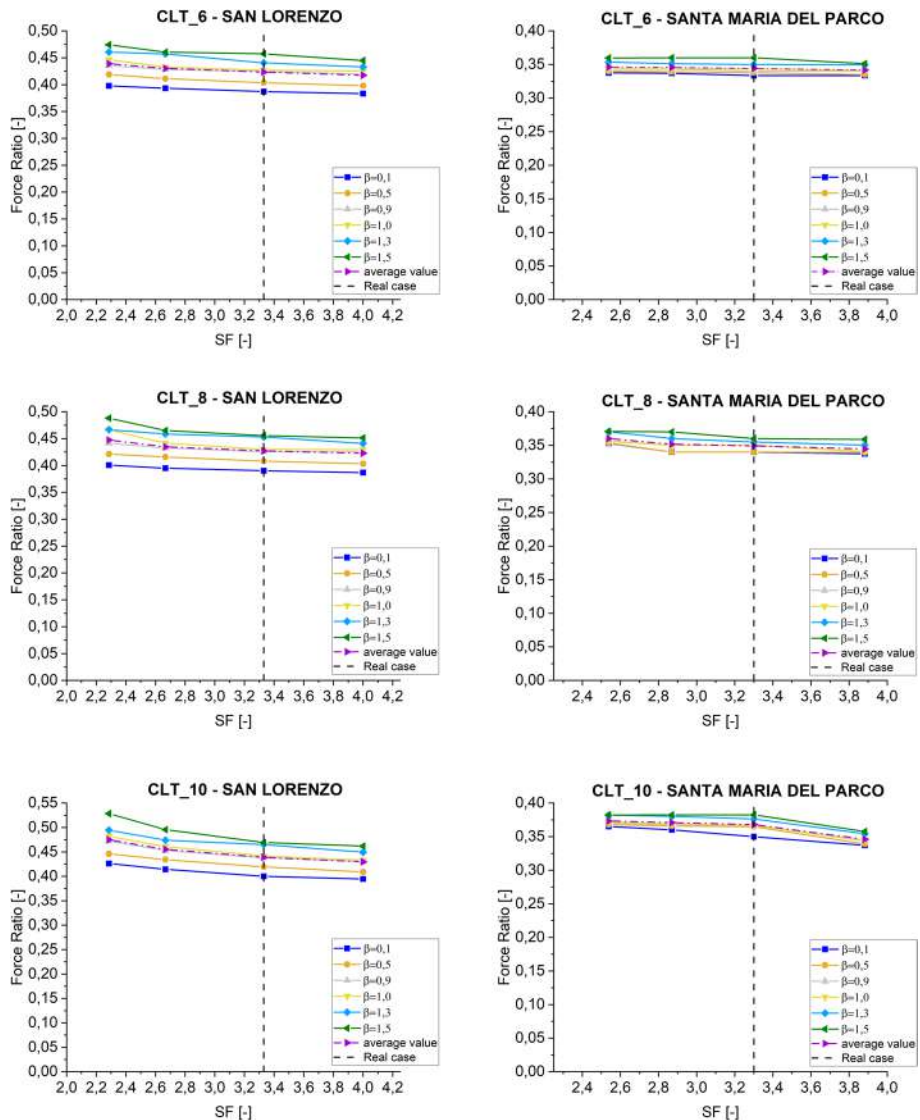


Fig. 24 Force ratio (base shear/axial load on the façade) for San Lorenzo and Santa Maria del Parco in relation to the shape factor (SF) for three different CLT roof structure configurations

Funding Open access funding provided by Politecnico di Milano within the CRUI-CARE Agreement. The authors have not disclosed any funding.

Declarations

Conflict of interest The authors have not disclosed any competing interests.

Open Access This article is licensed under a Creative Commons Attribution 4.0 International License, which permits use, sharing, adaptation, distribution and reproduction in any medium or format, as long as you give appropriate credit to the original author(s) and the source, provide a link to the Creative Commons

licence, and indicate if changes were made. The images or other third party material in this article are included in the article's Creative Commons licence, unless indicated otherwise in a credit line to the material. If material is not included in the article's Creative Commons licence and your intended use is not permitted by statutory regulation or exceeds the permitted use, you will need to obtain permission directly from the copyright holder. To view a copy of this licence, visit <http://creativecommons.org/licenses/by/4.0/>.

References

- Benedetti D, Castellani A (1981) *Costruzioni in zona sismica*. Masson Italia, Milano
- Betti M, Galano L, Vignoli A (2014) Comparative analysis on the seismic behaviour of unreinforced masonry buildings with flexible diaphragms. *Eng Struct*. <https://doi.org/10.1016/j.engstruct.2013.12.038>
- Betti M, Borghini A, Boschi S et al (2018) Comparative seismic risk assessment of basilica-type churches. *J Earthq Eng*. <https://doi.org/10.1080/13632469.2017.1309602>
- Bolis V, Giuriani E, Marini A, Perretti M, Preti M (2013) Coperture dissipative per il controllo del rocking degli archi diaframma nelle chiese tradizionali. Technical Report 13 – 2013 Department of Civil Engineering, Architecture, Land and Mathematics DICATAM – University of Brescia
- Brandonisio G, Mele E, Santaniello R, De Luca A (2008) Seismic safety of basilica churches: analysis of ten case studies. In: *Struct Anal Hist Constr Preserv Saf significance Proc Sixth Int Conf Struct Anal Hist Constr 2–4 July 2008*, Bath, United Kingdom
- CIRCOLARE 21 gennaio 2019, n. 7 C.S.LL.PP (2019). Istruzioni per l'applicazione dell'Aggiornamento delle "Norme tecniche per le costruzioni" di cui al decreto ministeriale 17 gennaio 2018
- Dal Cin A, Russo S (2016) Annex and rigid diaphragm effects on the failure analysis and earthquake damages of historic churches. *Eng Fail Anal*. <https://doi.org/10.1016/j.engfailanal.2015.09.010>
- De Matteis G, Zizi M, Corlito V (2017) Preliminary analysis of the effects of Centro-Italia earthquake on one nave Churches. *Atti del XVII Convegno ANIDIS L'ingegneria Sismica in Italia : Pistoia, 17–21 settembre 2017*
- Fazzi R, Galassi S, Misseri G, Rovero L (2021) Seismic vulnerability assessment of the Benedictine Basilica typology in central Italy. *J Build Eng* 43(2012):102897. <https://doi.org/10.1016/j.jobbe.2021.102897>
- Ferreira TM, Romeu V, Costa AA, Varum H (2014) Application of the trilinear model for the analytical study of the out-of-plane behaviour of unreinforced stone masonry walls. 9th international Masonry Conference 2014, Guimaraes
- Gavric I, Fragiaco M, Ceccotti A (2015) Cyclic behaviour of typical metal connectors for cross-laminated (CLT) structures. *Mater Struct Constr*. <https://doi.org/10.1617/s11527-014-0278-7>
- Genshu T, Yongfeng Z (2007) Seismic force modification factors for modified-Clough hysteretic model. *Eng Struct* 29:3053–3070. <https://doi.org/10.1016/j.engstruct.2006.12.007>
- Giuriani E, Marini A (2008) Wooden roof box structure for the anti-seismic strengthening of historic buildings. *Int J Archit Herit*. <https://doi.org/10.1080/15583050802063733>
- Giuriani E, Marini A, Preti M (2016) Thin-folded shell for the renewal of existing wooden roofs. *Int J Archit Herit*. <https://doi.org/10.1080/15583058.2015.1075626>
- Giuriani E, Marini A, Porteri C, Preti M (2009) Seismic vulnerability of churches associated to transverse arch rocking. *International Journal of Architectural Heritage*, 3: 1–24, 2009. Ed. Taylor & Francis Group, LLC
- Gubana A (2010) Experimental tests on timber-to-cross lam composite section beams. In: *Proc 11th World Conf Timber*
- Gubana A (2015) State-of-the-art report on high reversible timber to timber strengthening interventions on wooden floors. *Constr Build Mater*. <https://doi.org/10.1016/j.conbuildmat.2015.06.035>
- Gubana A, Melotto M (2018) Experimental tests on wooden-based in-plane strengthening solutions for the seismic retrofit of traditional timber floors. *Constr Build Mater* 191:290–299. <https://doi.org/10.1016/j.conbuildmat.2018.09.177>
- Hossain A, Lakshman R, Tannert T (2015) Shear connections with self-tapping screws for cross-laminated timber panels. *Conference ASCE Structures Congress*, Portland, Oregon. <https://doi.org/10.1061/9780784479117.195>
- Iervolino I, De Luca F, Cosenza E (2010a) Spectral shape-based assessment of SDOF nonlinear response to real, adjusted and artificial accelerograms. *Eng Struct*. <https://doi.org/10.1016/j.engstruct.2010.04.047>

- Iervolino I, Galasso C, Cosenza E (2010b) REXEL: Computer aided record selection for code-based seismicstructural analysis. Bull Earthq Eng. <https://doi.org/10.1007/s10518-009-9146-1>
- Iervolino I, Galasso C, Paolucci R, Pacor F (2011) Engineering ground motion record selection in the Italian ACcelerometric Archive. Bull Earthq Eng. <https://doi.org/10.1007/s10518-011-9300-4>
- Johansen KW (1949) Theory of timber connections, vol 9. IABSE Publications, pp 249–262
- Kita A, Cavalagli N, Venanzi I, Ubertini F (2021) A new method for earthquake-induced damage identification in historic masonry towers combining OMA and IDA
- Lagomarsino S, Penna A, Galasco A, Cattari S (2013) TREMURI program: an equivalent frame model for the nonlinear seismic analysis of masonry buildings. Eng Struct 56:1787–1799. <https://doi.org/10.1016/j.engstruct.2013.08.002>
- Larsen HJ (1977) Johansen's Nail Tests. Bygningssstatistiske Meddelelser 48:9–30
- Lee J, Fenves GL (2002) Plastic-damage model for cyclic loading of concrete structures. J Eng Mech. [https://doi.org/10.1061/\(asce\)0733-9399\(1998\)124:8\(892\)](https://doi.org/10.1061/(asce)0733-9399(1998)124:8(892))
- Longarini N, Crespi P, Franchi A et al (2018) Cross-lam roof diaphragm for the seismic retrofitting of historical masonry churches. In: Proceedings of the 10th International Masonry Society Conferences
- Longarini N, Crespi P, Scamardo M (2019). Numerical approaches for cross-laminated timber roof structure optimization in seismic retrofitting of a historical masonry church. Bull Earthq Eng Springer Nature B.V. 2019, <https://doi.org/10.1007/s10518-019-00661-w>
- Lourenço PB, Rots JG, Blaauwendraad J (1995) Two approaches for the analysis of masonry structures: micro and macro-modeling. Heron 40(4):313–340
- Lubliner J, Oliver J, Oller S, Oñate E (1989) A plastic-damage model for concrete. Int J Solids Struct. [https://doi.org/10.1016/0020-7683\(89\)90050-4](https://doi.org/10.1016/0020-7683(89)90050-4)
- Lucibello G, Brandonisio G, Mele E, De Luca A (2010) Seismic behavior of some Basilica Churches after L'Aquila 2009 Earthquake. Adv Mater Res. <https://doi.org/10.4028/www.scientific.net/amr.133-134.801>
- Marini A, Giuriani E, Belleri A, Cominelli S (2018) Dowel connections securing roof-diaphragms to perimeter walls in historic masonry buildings and in-field testing for capacity assessment. Bull Earthq Eng. <https://doi.org/10.1007/s10518-018-0333-9>
- Martinez G, Roca P, Clapes J (2006) Characterization of the dynamic response for the structure of mallorca cathedral—structural analysis of historical constructions, New Delhi 2006 P.B. Lourenço, P. Roca, C. Modena, S. Agrawal (Eds.)
- Mibact (2010) Linee Guida per la valutazione e la riduzione del rischio sismico del patrimonio Culturale – allineamento alle Nuove tecniche per le costruzioni” Ministero dei Beni e delle attività culturali
- Midas Midas (2021) GEN FX Program—general structure design system version v.2.1
- Milani G (2013) Lesson learned after the Emilia-Romagna, Italy, 20–29 May 2012 earthquakes: a limit analysis insight on three masonry churches. Eng Fail Anal. <https://doi.org/10.1016/j.engfailanal.2013.01.001>
- Milani G, Valente M, Alessandri C (2018) The narthex of the Church of the Nativity in Bethlehem: a non-linear finite element approach to predict the structural damage. Comput Struct. <https://doi.org/10.1016/j.compstruc.2017.03.010>
- NTC2018 (2018) Norme Tecniche per le Costruzioni. Ministero delle infrastrutture e dei trasporti. Supplemento ordinario n. 8 alla Gazzetta ufficiale Serie generale. n. 42
- Otani S (1981) Hysteresis models of reinforce concrete for earthquake response analysis. J Fac Eng 36:407–441
- Pagnoni T (1994) Seismic analysis of masonry and block structures with the discrete element method. In: 10th European conference, Earthquake engineering, pp 1674–1694
- Parisi MA, Piazza M (2015) Seismic strengthening and seismic improvement of timber structures. Constr Build Mater. <https://doi.org/10.1016/j.conbuildmat.2015.05.093>
- Pavia A, Scozzese F, Petrucci E, Zona A (2021) Seismic upgrading of a historical masonry bell tower through an internal dissipative steel structure buildings 2021, 11(1), 24 <https://doi.org/10.3390/buildings11010024>
- Preti M, Loda S, Bolis V et al (2017) Dissipative roof diaphragm for the seismic retrofit of listed masonry churches. J Earthq Eng. <https://doi.org/10.1080/13632469.2017.1360223>
- Preti M, Bolis V, Marini A, Giuriani E (2014) Example of the benefits of a dissipative roof diaphragm in the seismic response of masonry. In: Proc 9th Int Conf Struct Anal Hist Constr
- Rinaldin G, Amadio C, Fragiocomo M (2013) A component approach for the hysteretic behaviour of connections in cross-laminated wooden structures. Earthq Eng Struct Dyn. <https://doi.org/10.1002/eqe.2310>

- Roca P, Clemente R (2005) Studies on the origin of deformation and damage in long-span historical structures. 11th. International conference on fracture. Turin, Italy (Abstract Book and CD-ROM), p. 642. S. A. F
- Roensmaens B, Van Parys L, Branco J, Descamps T (2019) Proposal of a CLT reinforcement of old timber floors. In: RILEM Bookseries
- Roque J, Oliveira DV, Ferreira TM, Lourenco PB (2019) Nonlinear dynamic analysis for safety assessment of heritage buildings: church of Santa Maria de Belém. *J Struct Eng*, 145(12) 2019
- Sandhaas C, van de Kuilen JWG (2017) Strength and stiffness of timber joints with very high strength steel dowels. *Eng Struct*. <https://doi.org/10.1016/j.engstruct.2016.10.046>
- Sferrazza Papa G, Tadeo V, Parisi MA (2021) Casolo S (2020) Seismic response of a masonry church in Central Italy: the role of interventions on the roof. *Bull Earthq Eng* 19:1151–1179. <https://doi.org/10.1007/s10518-020-00995-w>
- Sorrentino L, Cattari S, Da Porto F, Magenes G, Penna A (2019) Seismic behaviour of ordinary masonry buildings during the 2016 central Italy earthquakes. *Bull Earthq Eng* 17:5583–5607
- Tomasi R, Crosatti A, Piazza M (2010) Theoretical and experimental analysis of timber-to-timber joints connected with inclined screws. *Constr Build Mater*. <https://doi.org/10.1016/j.conbuildmat.2010.03.007>
- Turrini G, Piazza M (1983) Una tecnica di recupero statico del solai in Legno TT—technique for static reinforcement of wooden beam floors. *Recuperare* 5:224–237
- Totani G, Monaco P, Totani F, Lanzo G, Pagliaroli A, Amoroso S, Marchetti D (2016) Site characterization and seismic response analysis in the area of Collemaggio, L'Aquila (Italy) Proc. 5 th International Conference on Geotechnical and Geophysical Site Characterization ISC'5, Gold Coast, Queensland, Australia, 5–9 September, Vol. 2, 1051–1056. B.M. Lehan, H.E. Acosta-Martínez and R. Kelly (eds). ISBN 978-0-9946261-2-7. Australian Geomechanics Society, Sydney, Australia.
- Valente M, Milani G (2018a) Damage assessment and partial failure mechanisms activation of historical masonry churches under seismic actions: three case studies in Mantua. *Eng Fail Anal*. <https://doi.org/10.1016/j.engfailanal.2018.06.017>
- Valente M, Milani G (2018b) Damage survey, simplified assessment, and advanced seismic analyses of two masonry churches after the 2012 Emilia earthquake. *Int J Archit Herit*. <https://doi.org/10.1080/15583058.2018.1492646>
- Valente M, Milani G (2018c) Seismic response and damage patterns of masonry churches: seven case studies in Ferrara. Italy *Eng Struct*. <https://doi.org/10.1016/j.engstruct.2018.08.071>
- Valente M, Barbieri G, Biolzi L (2017) Damage assessment of three medieval churches after the 2012 Emilia earthquake. *Bull Earthq Eng*. <https://doi.org/10.1007/s10518-016-0073-7>
- Valluzzi MR, Sbrogiò L, Saretta Y, Heisha V (2021) Seismic response of masonry buildings in historical centres Struck by the 2016 central Italy earthquake. Impact of building features on damage evaluation. *Int J Architectural Heritage Conserv, Anal, Restor* <https://doi.org/10.1080/15583058.2021.1916852>
- Zucca M, Franchi A, Crespi P, Longarini N, Ronca P (2018) The new foundation system for the transept reconstruction of the basilica di Collemaggio. Proceeding of the International Masonry Society Conference, Volume 0, Issue 222279, pp 2441–2450, 10th International Masonry Conference IMC 2018, Milan, 9–11 July 2018.
- Zucca M, Crespi P, Longarini N, Scamardo M (2020) The new foundation system of the Basilica di Collemaggio's transept. *Int J Masonry Res*. <https://doi.org/10.1505/IJMRI.2020.104896>